KTH Engineering Sciences

Simulation of Rail Wear on the Swedish Light Rail Line Tvärbanan

by

Anneli Orvnäs

TRITA AVE 2005:12
ISSN 1651-7660
ISRN KTH/AVE/RTM-05/12-SE

Postal Address
Royal Institute of Technology
Aeronautical and Vehicle Engineering
Railway Technology
SE-100 44 Stockholm

Visiting address
Teknikringen 8
Stockholm

Telephone
+46 8 790 84 76
Fax
+46 8 790 76 29

E-mail
mabe@kth.se

Preface

This thesis work is part of my Master of Science degree and is carried out in collaboration with SL (Stockholm Transport) and the Division of Railway Technology, Department of Aeronautical and Vehicle Engineering at the Royal Institute of Technology (KTH) in Stockholm.

I would like to thank my supervisor at KTH, Roger Enblom, for his good support and guidance during this work. I am also grateful for the help I have received from my supervisor and examiner Mats Berg.

I also would like to show my gratitude to my supervisors at SL, Ulf Bik and Faegh Adelpour, who have provided me with all the necessary data for this work.

I am very grateful to Ingemar Persson at DEsolver, who always has been ready to help me with my questions and inquiries regarding the simulation software.

Thanks to all colleagues at the division and especially to my room mate Nizar Chaar, who has helped and inspired me in my work.

Last, but not least, I would like to thank my dear Lena, who has supported me and given me linguistic advice to this report.

Stockholm, March 2005

Anneli Orvnäs

Abstract

Rail wear can result in extensive costs for the track owner if it is not predicted and prevented in an efficient way. To limit these costs, one measure is to predict rail wear through wear simulations.

The purpose with this work is to perform simulations of successive rail wear on the Swedish light rail line Tvärbanan in Stockholm, by means of the track-vehicle dynamics software GENSYS in combination with a wear calculation program developed in MATLAB.

The simulation procedure is based on a methodology with a simulation set design, where the simulations to be performed are selected through a parametric study. The simulations include track-vehicle simulations, where the wheel-rail contact is modelled according to the Hertzian contact theory together with Kalker's simplified theory (including the numerical algorithm FASTSIM). The results from the track-vehicle simulations serve as input to the wear calculations.

When modelling rail wear Archard's wear model has been used, including wear coefficients based on laboratory measurements. The measurements have been performed under dry conditions, so the wear coefficients under lubricated conditions (both natural and deliberate lubrication) are reduced by factors estimated by field observations.

After the wear depth calculations the wear distribution is smoothed and the rail profile is updated. The simulation procedure continues with a new wear step as long as the desired tonnage is not attained.

Four curves of Tvärbanan with different curve radii, ranging from 85 to 410 m, have been studied in this work. On three of the curves the high rail is deliberately lubricated, whereas no lubrication has been applied in the widest curve. The vehicle operating the light rail line is an articulated tram with two motor end bogies and one intermediate trailer bogie.

The line was opened in August 1999 and extended in one direction one year later. Rail profile measurements have been carried out by SL since March 2002. The traffic tonnage at the selected sites from the opening of the line to the last measurement occasion (September 2004) is at most 8.9 mega gross ton per track.

The results of the rail wear prediction tool are evaluated by comparing worn-off area of the simulated rail profiles with that of the measured rail profiles. Simulated and measured results do not agree too well, since the simulated rail wear is more extensive than the measured one, especially on the outer rail. However, the shapes of the simulated worn rail profiles are comparable to those of the measured rail profiles.

Contents

1 Introduction

Railway technology is developing towards increased axle loads and higher speeds, which usually leads to increased stresses and strains of the rails. Despite considerable improvements of rail materials in recent years, the dynamic interaction between wheel and rail continues to cause significant wear, which results in extensive costs. To limit these costs, one measure that can be taken is to perform wear prediction through simulations, which can improve maintenance planning and optimize service procedures.

Wear, in this context, means material removal from the rail. Rail wear can be divided into two different types; mild and severe. Mild wear often results in a smoother surface than the original one, whereas severe wear often causes a rougher surface. Rail wear is dependent on vehicle-track dynamics, contact mechanics and tribology. Other types of damage of the rail are plastic deformation, surface cracks, corrugation and fatigue. It is, however, only the change of the rail profile caused by material removal that will be regarded in this work.

Figure 1-1 shows an illustration of rail profiles measured at Tvärbanan (the present case study) on different occasions, which have been exposed to different amounts of traffic load and thus have different shape due to wear. The measurements have been performed at the same measuring site over a period of two and a half years and are compared to a nominal BV50 rail profile.

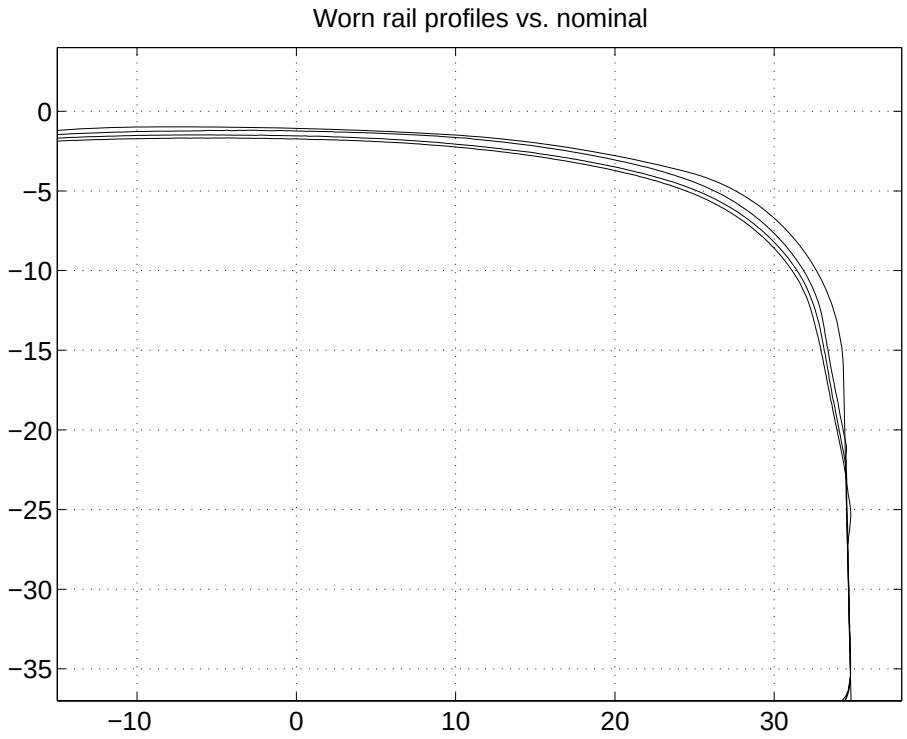

Figure 1-1 Rail profiles from three measurements during two and a half years compared to a nominal BV50 rail profile. *Gauge side of a high rail.*

1.1 Background

By observing the rail wear distribution along a railway track it can be noticed that the major part of the wear occurs in sharper curves, in the first place on the outer rail, which is also referred to as the high rail. The rail wear rate seems to increase exponentially with a decrease in curve radius, both for high and low rails (given that there is no man-made lubrication). The rail wear rate is, however, typically 6-7 times higher for the high rail than for the low rail [18]. The wear rate of the rail is thus strongly influenced by the curve radius and also by contact pressure in the contact area. The microstructure and hardness of the materials, as well as temperature, also affect the wear rate.

In order to reduce the most severe rail wear, lubrication of the high rail for the most wear exposed curves can be introduced. The reduction is, however, dependent on the distance from the trackside lubricating device. Weather conditions can also be a wear reducing factor, since precipitation has a lubricating effect. On the other hand, high air temperature has the opposite effect, since oil in the lubricant evaporates and the lubrication effect is reduced [18].

Modifications of the vehicles can also reduce the wear rate; radial steering running gear, with soft horizontal suspension, generates less wear on both wheel and rail. This is achieved when the yaw angle of the wheelset relative to the track is small and the wheelset axle is pointing towards the centre of the curve. On the other hand, the radial steering vehicle loses some of its running stability on straight track, which results in a decrease of its critical speed.

A railway vehicle needs wheel-rail contact forces, partly tangential, partly normal, to support the vehicle and to have the ability to accelerate, brake and negotiate curves of the track. The tangential forces in the contact plane are transmitted through a certain amount of friction in the contact zone, which is divided into stick and slip regions. High contact stresses in this zone can cause plastic deformation. How much material that is deformed depends on the hardness of the rail, traffic load and curve radius. Friction forces, also called creep forces, arise due to small sliding motions between wheel and rail. Acceleration and braking of the vehicle increases the longitudinal creep forces, which leads to higher wear rate. The contact forces will be explained in more detail in Chapter 2.

Work on predicting rail profile wear by computer simulations has not yet come so far as the corresponding work on the wheels. Therefore, it is of special interest to find a wear predicting tool considering rail wear that agrees with reality as much as possible, so that rail wear can be reduced in a more efficient way. Previous work in the area has been performed by particularly Enblom [7], [8] and Zobory [24].

1.2 Purpose and scope of this work

This study will concentrate on tracks of the Swedish light rail line Tvärbanan, located in Stockholm. Measurements of rail profiles have been carried out in three different curves of the line during the period March 2002 to September 2004, and in this study they are compared with simulated results of rail wear. A fourth curve was added as measuring site in November 2003. The rail wear simulations in this work are performed with the vehicle-track dynamics software GENSYS [6] in combination with a wear calculation program developed in MATLAB [23].

Thesis contents

In the next chapter the general simulation procedure will be presented. The wheel-rail contact problem, which can be regarded as a normal and a tangential contact problem, will also be described. Furthermore, it also treats the current wear model and some important factors valid for the model. This will be followed by a description of the case study of Tvärbanan in Chapter 3, where the track, the current measuring sites and the vehicle will be introduced. Chapter 4 describes how the track and vehicle have been modelled for the simulations. The rail wear results of the comparison between the simulations and the measurements will be presented in Chapter 5, followed by a sum up of conclusions and suggestions of future work in Chapter 6.

2 Methodology

This chapter first describes the proposed rail wear simulation procedure. Then a general presentation of the phenomena creepage and spin that arise in the contact area between wheel and rail during rolling motion is given, as well as a survey of the contact problem's division into normal and tangential components. Furthermore, wear modelling will be explained, going into more details with Archard's wear model, wear coefficients and wear maps. Most of the information in sections 2.2 and 2.3 has been found in [1] and in [12].

2.1 Wear simulation procedure

The idea with the proposed simulation procedure is that the methodology can be applicable to an arbitrary simulation case of successive rail wear. The methodology is illustrated in the flow chart in Figure 2-1.

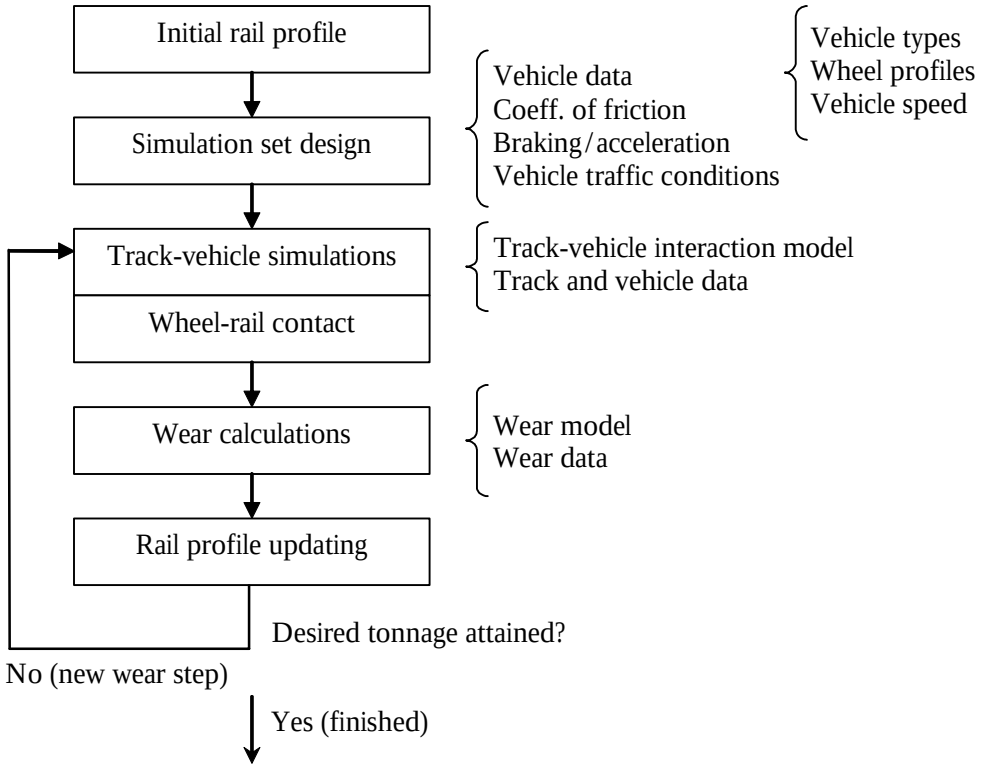

Figure 2-1 Flow chart of the methodology for rail wear simulation.

The rail wear simulation is started with an initial rail profile of the track that is to be evaluated. The simulation set, or load collective, describes the traffic the track in question will be exposed to, including the most interesting parameters for the wear simulations, such as vehicle types, wheel profiles, vehicle speed, coefficient of friction and braking/ acceleration. The choice of simulation set may be supported by a parametric study, where the parameters are varied and considered to what extent they should be used. The purpose with a parametric study is to limit the number of simulations and thus save simulation time. Once the simulation set has been chosen it is kept constant throughout the rail wear simulations.

The track-vehicle simulations are based on models of the track and vehicle, determined by the necessary track and vehicle data, as well as modelling of the wheel-rail contact. Contact forces are calculated and serve as input to the wear calculations, where a specific wear model is defined. The theory behind wheel-rail contact modelling and the present wear model will be described in the following sections. After the wear depth calculations the wear distribution is smoothed and the rail profile is updated. The simulation procedure restarts with the updated rail profile as input as long as the desired tonnage is not attained. Each iteration is called a *wear step* and is limited by conditions on wear depth and axle passages per step.

2.2 Wheel-rail contact modelling

2.2.1 Creepage and spin

Generally, the wheels do not perform a pure rolling motion on the rails, but give rise to creepage (or sliding) and spin in the contact area between wheel and rail. Creepage and spin are in turn the cause of creep forces, also called friction forces, and spin moments. The size of these forces depends on the magnitude of the creepage and spin. Apart from creepage and spin, the friction forces are also functions of wheel-rail geometry, material properties, the coefficient of friction and normal forces [11].

The sliding motion is divided into three components; in travelling (longitudinal) direction, transversal (lateral) direction and rotation about an axis perpendicular to the contact area. Creepage and spin in all three directions, which depend on sliding velocities and angular sliding velocity, have a great influence on the size of the creep forces.

Sliding velocities, creepage and creep forces are described through a coordinate system locally for the contact area with the three directions ξ - η - ζ, where ξ is defined positive in the rolling direction, η is in the contact plane and perpendicular to the travel direction and ζ is perpendicular to the contact plane. The coordinate system is shown in Figure 2-2.

Creepages in the longitudinal and lateral directions (υ_ξ, υ_η) are defined as the average sliding velocities (v_ξ and v_η) normalized by the vehicle speed ($v_{vehicle}$). Spin (ϕ), on the other hand, is defined as the angular sliding velocity (ω) normalized by the vehicle speed. The total creepage, υ, is a vectorial sum of the longitudinal and the lateral creepages. Thus

$$\textit{Longitudinal creepage} \quad \upsilon_\xi = \frac{v_\xi}{v_{vehicle}} \quad [-] \qquad (2\text{-}1)$$

$$\textit{Lateral creepage} \quad \upsilon_\eta = \frac{v_\eta}{v_{vehicle}} \quad [-] \qquad (2\text{-}2)$$

$$\textit{Spin creepage} \quad \phi = \frac{\omega}{v_{vehicle}} \quad [1/m] \qquad (2\text{-}3)$$

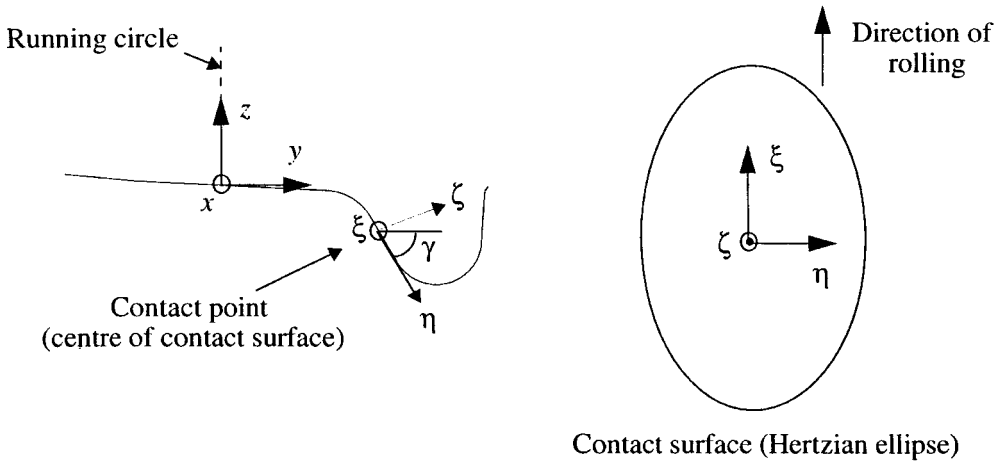

Figure 2-2 Coordinate system for the wheel profile (x-y-z) and for the contact surface (ξ - η - ζ) [12].

2.2.2 Normal contact problem

The wheel-rail contact problem is a very complex and time demanding operation by simulation work, which requires high computer capacity. In order to solve the contact problem more easily it can be regarded as partly a normal, partly a tangential contact problem. The normal and tangential forces are, however, dependent on and influenced by each other, but in order to be able to treat the normal and the tangential contact problem seperately the Hertzian contact theory is used [10]. It consists of the following assumptions and approximations:

- Deformations are small and the materials in contact have linear elastic behaviour.
- The contact area is small in comparison with typical dimensions of the bodies in contact, e.g. the wheel radius, which leads up to a half-space assumption[1)].
- The curvatures of the bodies in contact are constant in and near the contact area in order to be able to calculate its shape and size.
- The surfaces are ideally smooth.
- The materials of the bodies are homogenous and isotropic (same properties in all directions).
- The bodies are quasi-identical (geometrically and elastically the same), which implies that the normal and tangential contact problems can be treated separately.

According to Hertz' contact theory the contact between wheel and rail can be regarded as a contact area of elliptical shape. The size of the contact ellipse depends on the normal load and the geometry of wheel and rail and is defined by the semi-axes *a* and *b*. The contact pressure within the contact area is distributed according to Figure 2-3.

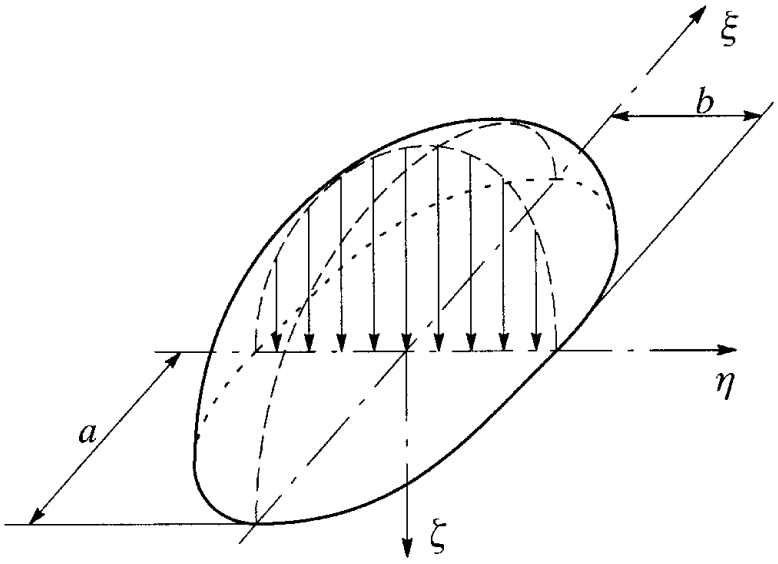

Figure 2-3 Distribution of the contact pressure within the Hertzian elliptical contact area [1].

Hertz' contact theory can sometimes be considered to be too simplified and approximate compared to reality. Especially the half-space assumption is generally not valid when the contact area is located at the gauge corner of the rail and thus the flange of the wheel. It is,

1) The half-space assumption implies that the bodies in contact are regarded as semi-infinit bodies limited by a plane surface [1].

however, the most commonly used theory due to its relatively short calculation times. Non-Hertzian theories with non-elliptical contact areas are much more complex and not readily available and are thus not usable for the present study.

2.2.3 Tangential contact problem

Creep forces are, as already mentioned, functions of creepage and spin in the contact area and arise in the tangential plane. The resulting creep force is a non-linear function of the creepage, with a maximum value of μN. The problem can, however, be regarded as linear when the creepage is assumed to be small (near origin), which can be seen in Figure 2-4. When there are no creepage or spin there are also no friction forces.

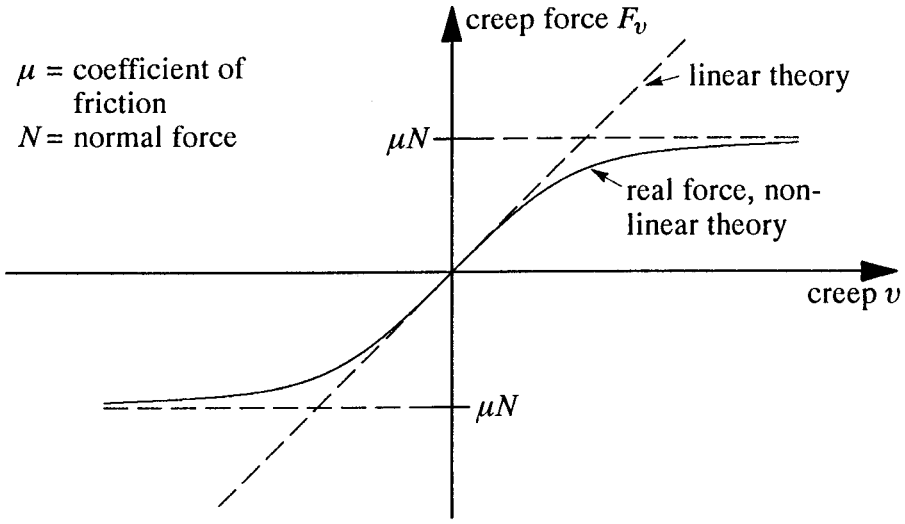

Figure 2-4 Creep force as function of creepage (one-dimensional case) [1].

Apart from the approximations valid for the normal contact problem, some assumptions can be supplemented to be valid also for the tangential contact problem:

- Inertia forces can be neglected.
- Stationary contact is prevailing.
- There is a dominant speed direction in the contact area that coincides with one of the axes of the coordinate system of the contact area.
- The coefficient of friction is constant.

The contact area can be divided into an adhesion region and a slip region. When the developed creep force is less than the coefficient of friction (in the ξ- and η-direction) times the normal force, sliding occurs only in a part of the contact area. But when the resultant force in the contact plane equals μN there will be a pure sliding motion. See Figure 2-5.

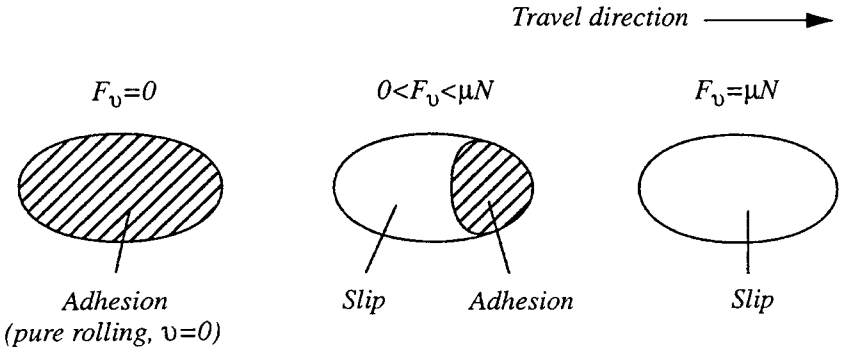

Figure 2-5 Adhesion and slip regions of the contact area. *F_υ = total creep force in the contact area, μ = coefficient of friction, N = normal force [11].*

Different theories for calculating the friction forces

There are a number of different theories for the solution of the tangential contact problem. The basic and most simple one is *Kalker's linear theory* [15], which calculates creep forces and spin moment as functions of small creepages and spin. However, the approximation with linear relations is a limitation, since the theory practically is valid only for minimal motions on straight track and ideal conditions in curves.

Kalker's linear theory has served as starting point for more or less exact non-linear theories, for example the one developed by Shen, Hedrick and Elkins [22]. Also Kalker has developed a non-linear and more accurate theory, regarded as a complete theory, which is able to calculate creep forces even outside the linear region [14][15][16]. The disadvantage of this theory is, however, that the numerical solutions are very time consuming.

A middle course between the linear and non-linear complete theory is *Kalker's simplified theory* [14][17], which is commonly used for modelling the tangential contact between wheel and rail. It is a non-linear theory, describing the most important phenomena in a rather precise way, but still requiring less computer time than the non-linear complete theory. A numerical algorithm called FASTSIM [14] is used together with Kalker's simplified theory. FASTSIM calculates the pressure distribution and creep forces in the contact area, with the solution of the normal contact problem as input data. Furthermore, the output data here serve as input to a wear model that will be explained later in this chapter. In comparison with the complete theory, the simplified theory implements calculations approx. 1000 times faster with a maximum deviation of at most 15 % [1].

The difference between the simplified and the complete theory consists of how the deformation is regarded. In the complete theory the deformation in one point depends on the loads in all points nearby. In the simplified theory, on the other hand, the rail is modelled as a bed or "mattress" of springs that deform individually, i.e. the deformation in every single point depends only on the load in this specific point. This is called the *Winkler method*, or elastic foundation method, and can be observed in Figure 2-6.

In the present case study the contact problem is solved according to Hertz' theory for the normal contact problem together with Kalker's simplified theory for the tangential contact problem. Zobory that also has performed rail wear simulations utilizes, on the other hand, the Hertzian theory in combination with Kalker's linear theory [24].

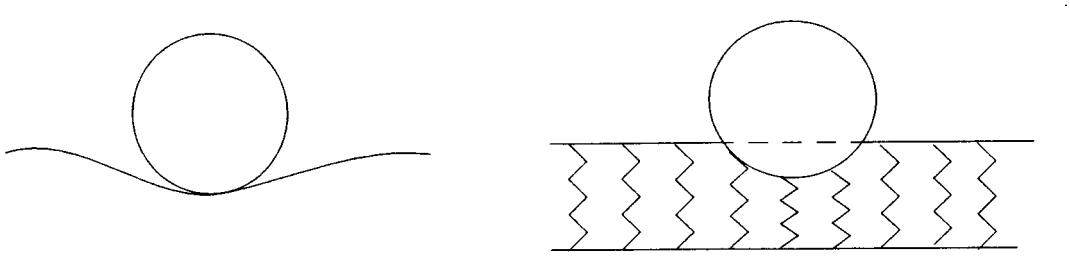

Figure 2-6 ***The complete and the simplified theory.*** *In the simplified theory (Winkler method) all deformations outside the contact area disappear, since deformation occurs only where the two bodies are in contact [1].*

2.3 Wear modelling

Wear prediction requires a wear model, which takes the material properties and the quantities in the wheel-rail contact in consideration to describe the wear depth distribution over the rail profile. The most widely accepted wear model in the tribological society, and the one used in the present case study, is Archard's wear model that is presented briefly in this part of Chapter 2.

The wear rate describes how much material that has been removed and how fast the loss of material is progressing. As has been mentioned in the introductory chapter, wear is divided into mild and severe wear. Within the region of mild wear, the wear process is slow and can for example be represented by oxidation wear, generally present on the rail crown. The wear process in the region of severe wear is, on the other hand, much faster and corresponds to for example adhesive wear, generally present on the rail gauge face in sharper curves.

2.3.1 Archard's wear model

A wear model describes the loss of material, here on rails, through an equation or a set of equations. There is a vast number of different wear models developed, but they are all approximate to a certain extent. Archard's wear model is sufficiently accurate and makes it possible to model wear due to sliding [2].

According to this model the volume of wear is proportional to the wear coefficient k, the normal force N and the sliding distance s, and inversely proportional to the hardness H of the softer material in the contact. Neither the coefficient of friction nor the friction force are explicitly included in this equation, but are, nevertheless, related to some of the current parameters. The volume of wear according to Archard is defined as:

$$V_{wear} = k\frac{Ns}{H} \tag{2-4}$$

where V_{wear} is the volume of wear (m^3)

k is the wear coefficient (-)

N is the normal force (N)

s is the sliding distance (m)

H is the hardness of the softer material (N/m^2)

2.3.2 Wear coefficient and wear maps

The wear coefficient k is a very complex parameter to determine, since it varies considerably depending on sliding velocity, v_{slip} , and contact pressure, p, as well as on temperature and the degree of lubrication in the contact area [12]. In order to apply a reasonably adequate wear coefficient for the current wear simulations *wear maps* can be utilized. They describe the wear coefficient as function of sliding velocity and contact pressure and can in principle only be determined by laboratory measurements. Every wear map corresponds to a specific wheel/rail material combination (wheel and rail are assumed to have typically similar material properties) and to a specific lubrication condition, if any.

The wear map shown in Figure 2-7 describes four approximate regions, in which the wear coefficient varies within certain spans. The calculations are, however, further simplified in the present work by assuming a constant wear coefficient within each region. Specific regions where tread and flange contacts occur are also indicated in the wear map.

As can be seen in Figure 2-7 the contact pressure limit at $0.8H$ corresponds to 80% of the hardness, under which the wear coefficient depends merely on the size of the sliding velocity. In the first region, for low sliding velocities, the wear coefficient is rather low. In the region between 0.2 and 0.7 m/s the wear coefficient increases. As the sliding velocity approaches and exceeds 0.7 m/s the wear coefficient, however, decreases to the initial low level. Above the limit of $0.8H$ the wear coefficient is 10 times the highest value below the limit, which makes the wear conditions catastrophic and seizure occurs.

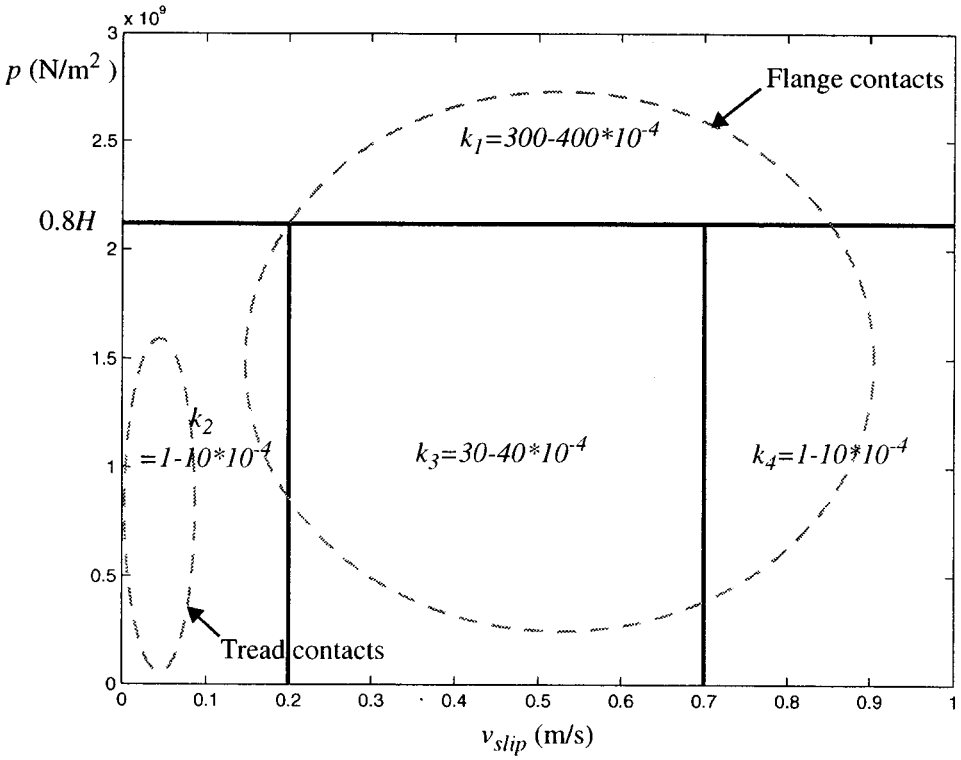

Figure 2-7 Wear map, valid for dry contact, with typical regions of tread and flange contact [12].

In the algorithm FASTSIM (mentioned in the previous section) the contact ellipse, at any instant of time and at any wheel-rail contact, is divided into a certain number of elements and it is determined whether an element belongs to the slip or adhesion zone of the contact ellipse. In each element the following quantities must be known in order to be able to determine the amount of wear:

- Hertzian contact pressure, p ($\mathrm{N/m^2}$)
- Wheel-rail sliding velocity vector, $\boldsymbol{v}_{slip}$ (m/s)
- Sliding distance, s (m)

According to Archard's wear equation (2-4) it is only the elements in the slip zone that contribute to the wear. The Hertzian contact pressure in each element is already known, but the sliding velocity and slidning distance must, however, be computed. The wear depth is calculated by applying Archard's wear equation locally to each element, divided by the area of the same element. Thus

$$\Delta\zeta = k\frac{p\Delta s}{H} \tag{2-5}$$

where $\Delta\zeta$ and Δs are the wear depth and the sliding distance in a certain contact element. The other variables have already been defined. The total amount of wear per contact occasion is then obtained by integrating the wear depth longitudinally in the slip zone area. Figure 2-8 illustrates the sliding velocity vector for a certain element inside the slip zone of the contact ellipse. The sliding velocity vector depends on creepage, spin and elastic surface deformation and can be defined as:

$$\begin{bmatrix} v_\xi \\ v_\eta \end{bmatrix} = v_{vehicle}\begin{bmatrix} \upsilon_\xi - \phi\eta - \dfrac{\partial u_\xi}{\partial\xi} \\ \upsilon_\eta + \phi\xi - \dfrac{\partial u_\eta}{\partial\xi} \end{bmatrix} \tag{2-6}$$

where $v_{vehicle}$ is the vehicle speed (m/s)

υ_ξ and υ_η are the longitudinal and lateral creepages in the contact area (-)

ϕ is the spin (1/m)

ξ and η are the local coordinates in the contact area (m)

u_ξ is the longitudinal elastic displacement in the contact area (m)

u_η is the lateral elastic displacement in the contact area (m)

The last term in the equation is thus a contribution to the sliding velocity from the elastic surface deformation. In a pure sliding contact area the term can be neglected, since it does not particularly affect the average sliding velocity. However, for contact areas only partly constituted by a slip region it contributes to a higher average of the sliding velocity. The elastic displacement contribution is chosen to be neglected in [12], but in [8] it is included in the calculation of the sliding velocity.

Once the resulting sliding velocity, v_{slip} , has been calcutated, it can be multiplied with the time each contact area element is in contact with the rail, Δt, in order to calculate the sliding distance in each element, Δs. The sliding velocity also affects the wear coefficient k in equation (2-5) according to the wear map of Figure 2-7.

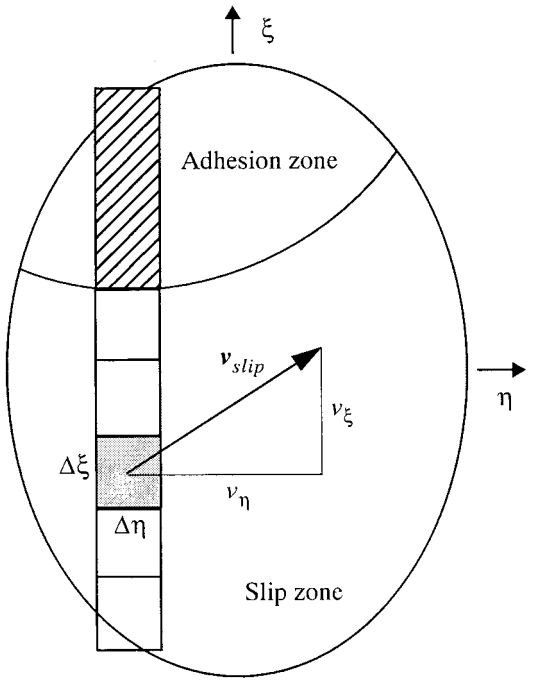

Figure 2-8 Definition of quantities in a contact ellipse. *The sliding velocity vector* $\mathbf{v}_{slip}$ *for a certain element of the slip zone is shown [12].*

Compensation of the wear coefficient

Wear prediction is a difficult task since the contact environment between wheel and rail varies considerably along the track and from time to time. The magnitudes of the wear coefficient given in Figure 2-7 are results from laboratory measurements under dry conditions. Since factors like weather phenomena, man-made lubrication and contamination change the conditions in the wheel-rail contact and thus affect the wear coefficient, it has to be compensated (reduced) to match these conditions. Some assumptions may, however, be made when reducing the wear coefficient [12]:

- Even during non-dry contact environment the regions in the wear map have the same limits as during dry conditions, whereas all wear coefficients are lowered by the same factor.
- The changing weather over time can be neglected and the values of the wear coefficient can thus be regarded as average values.
- The values of the wear coefficient are further scaled down for high rails in sharp curves if lubrication devices are active.

3 Case study

In this chapter the track, vehicle and traffic conditions for the present case study, Tvärbanan, are described. Since the focus of this work lies on the wear of the rail, firstly, the conditions for the track, measuring sites and rail profile will be introduced. Secondly, vehicle data including the wheel profile will be presented.

Rail wear is a process depending on the dynamic interaction between track and vehicle. In order to perform wear simulations correctly, it is of great importance to have access to all the required data for the track and vehicle. Some of the information regarding the track and vehicle has been received from [19] and [20].

3.1 Track and traffic conditions

The first part of Stockholm's light rail line Tvärbanan was opened in August 1999, connecting the stations Gullmarsplan and Liljeholmen, introducing a new type of vehicle, A32, which will be described later in this chapter. The line was extended one year later with tracks from Liljeholmen to Alvik. Another three years later, 2003, a line between Gullmarsplan and Sickla Udde was built. The present double track line (2005) thus runs from Alvik to Sickla Udde, a distance of 13 km (see Figure 3-1), with future plans of expansion in both ends. The major part of the line is situated on its own embankment, but to some extent it also runs among road traffic, which means that it is bound to normal traffic regulations.

3.1.1 Measuring sites

Four different sites along the track were selected for this study because of their location in sharper curves on the specific embankment, i.e. not among road traffic. On three of the curves (sections km 2+220, km 2+970 and km 10+610), rail profiles have been measured at six occasions since March 2002, whereas the fourth (section km 10+450) only is measured three times since November 2003. The curve radii vary from 85 to 410 metres for the measuring sites. More specific information for each site can be seen in Table 3-1. Profiles of both outer (high) and inner (low) rails are measured at all sites. In this work it has been chosen only to consider the sections of the northern track, i.e. the direction of travel from Sickla Udde to Alvik.

The entire light rail line and the selected measuring sites can be seen in Figure 3-1.

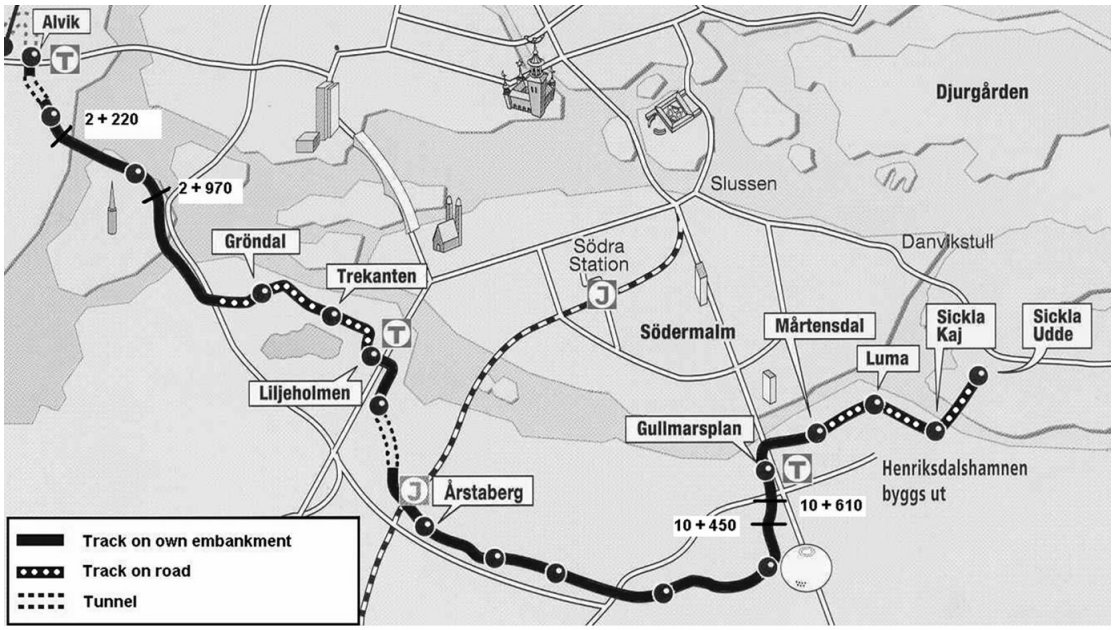

Figure 3-1 The entire light rail line Tvärbanan (2005) with the selected measuring sites.

Table 3-1 Track data for each measuring site of Tvärbanan (northern track).

Measuring sites	**2+220**	**2+970**	**10+450**	**10+610**
Radius (m)	300	130	410	85
Cant (mm)	76	72	25	39
Gradient (‰)	5	10	35	35
Track gauge[1)] (mm)	1440	1440	1440	1443
Rail fastening	Pr 401A	Pr 401A	Pr 1809	Pr 1809
Rail pad thickness (mm)	10	10	12	12
Distance after lubrication device[2)] (m)	186	56	-	43
Vehicle speed (km/h)	50	50	50	30
Traffic start	Aug. 2000	Aug. 2000	Aug. 1999	Aug. 1999
First measurement occasion	Mar. 2002	Mar. 2002	Nov. 2003	Mar. 2002

1) As measured in September 2004. Nominal track gauge is 1435 mm.

2) High rails only.

Lubrication

In order to decrease the wear rate on both rails and wheels, the gauge face of the high rail is lubricated in all curves with $R \leq 300$ m along the track. The lubricating device, which can be seen in Figure 3-2, is based on a box attached to the rail, containing an oil-based lubricant. From the box, a piece of felt is connected to the rail, which has been ground to a slightly concave form, where the felt is fitted. The felt absorbes the lubricant, which is being transmitted and spread along the curve by the passing wheels. The lubricating box is located 2-5 metres after the beginning of the transition curve and gives a lubricating effect up to several hundred metres. However, the effect decreases as a function of the distance after the lubricating device [18].

Figure 3-2 The lubricating device used at the embankment tracks of Tvärbanan. *Photo by Faegh Adelpour.*

Traffic conditions

A32 is the only vehicle type that operates on this light rail line, which simplifies the simulation modelling, since parameters from only one single vehicle must be taken into account. The number of vehicles used for maintenance of the track is considered to be small enough to be neglected. Table 3-2 shows the actual traffic tonnage for each site and year, from the opening of the line to the last measurement occasion (September 2004). The traffic tonnage is expressed in MGT, i.e. mega gross ton, and is summarized in the rightmost column of the table.

Table 3-2 The actual traffic tonnage (MGT per year and track) for each site, yearly and summarized, from August 1999/2000 to September 2004.

Measuring sites	**1999**	**2000**	**2001**	**2002**	**2003**	**2004**	**Σ**
2+220	-	0.7	1.6	1.9	2.1	1.5	**7.8**
2+970	-	0.7	1.6	1.9	2.1	1.5	**7.8**
10+450	0.4	1.4	1.6	1.9	2.1	1.5	**8.9**
10+610	0.4	1.4	1.6	1.9	2.1	1.5	**8.9**

3.1.2 Rail profile and material

The track at all the selected measuring sites consists of the rail type BV50, which is shown in Figure 3-3. It is a commonly used rail for this kind of light rail traffic. Each rail inclines with a certain angle towards the centre of the track, which provides an appropriate fit with the geometry of the conical-shaped wheels and hence enables a desirable transmission of vehicle load to the track. The nominal inclination of the present rails is 1:40 (about 1.5°). The rail consists of the same steel grade along the entire track, namely UIC 900A [4]. They are fastened to concrete sleepers with a sleeper distance of 0.80 m.

Note that the wheels also meet two types of grooved rails, namely R60N and G56 [19], on the parts of Tvärbanan that are integrated with the road traffic. Thus, they are not present for the selected measuring sites.

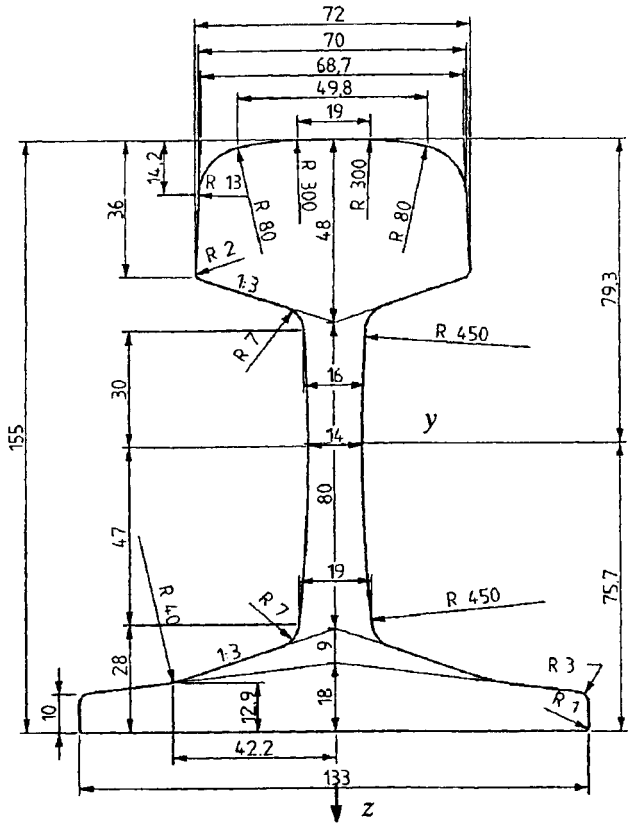

Figure 3-3 BV50 nominal rail. *Measures in mm.*

Rail profile measurements

The measurements at the light rail line Tvärbanan have been carried out by SL. The measuring device MINIPROF [9] has been used in order to document the successively worn rail profiles, see Figure 3-4. It consists of a measuring head that is fixed onto the rail head that is to be measured by a flat and strong magnet. The measuring element is a magnetic wheel, rolled manually over the rail surface, that is connected to the measuring head by a short two-part linkage. A long and stiff telescope rod is connected to the measuring head with a positioning pin at the other end of the rod that can be fixed to the opposite rail. Hence, a measuring plane parallel to the track plane is obtained, which accomplishes a fix orientation in the roll direction. The MINIPROF device is linked to a computer that stores all the measuring data. Each measuring section is marked on the rail in order to secure that the same sections are being observed at every measurement occasion.

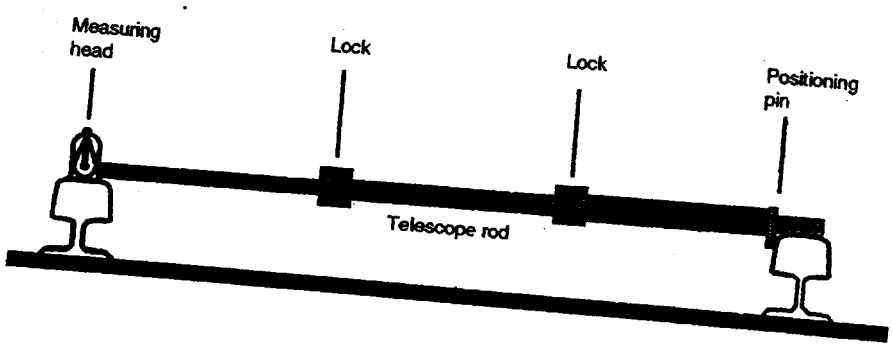

Figure 3-4 The MINIPROF measuring device [9].

In order to be able to observe how the rail is worn after different amounts of traffic tonnage, the measured rail profiles are compared with the nominal rail profile. Measured rail profiles at the site between Globen and Gullmarsplan (section km 10+610) at the northerly track, together with the nominal profile for rail BV50 are shown in Figure 3-5 as an example. The curve radius is 85 m. Figure 3-6 shows the corresponding rail profiles at section km 10+450, where the curve has a radius of 410 m. The measured rail profiles are a result of the latest measurement (September 2004), five years after the opening of Tvärbanan.

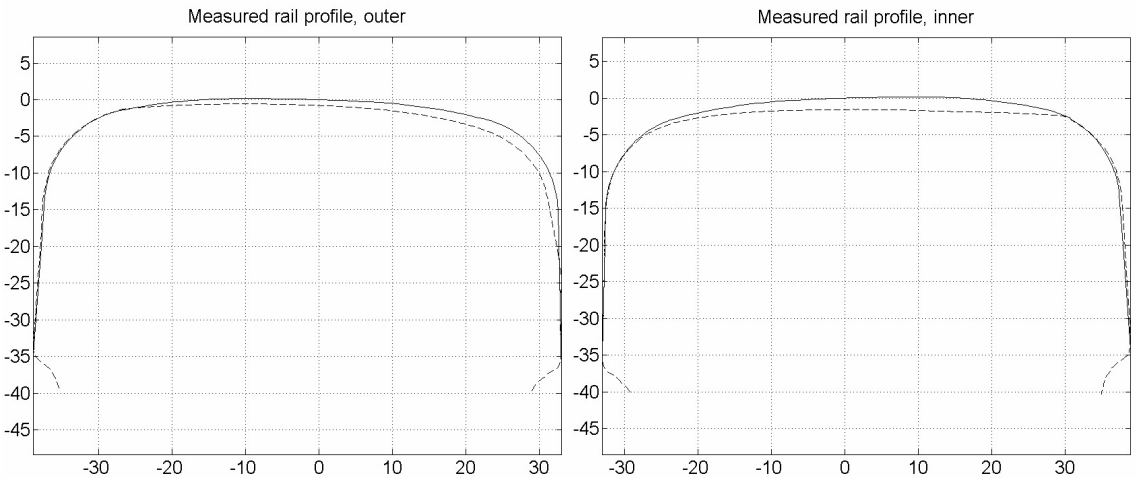

Figure 3-5 Measured rail profiles at section km 10+610, between Globen and Gullmarsplan, together with the nominal BV50 rail profile, inclined 1:40. *A period of five years, corresponding to a traffic volume of 8.9 MGT, have passed between the two profiles. The radius is R=85 m. The outer rail is lubricated.*

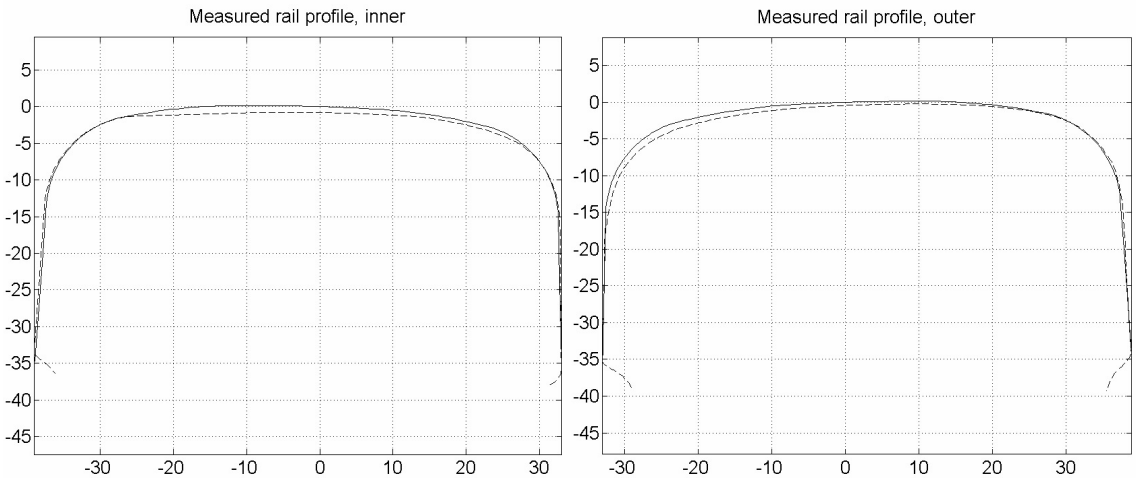

Figure 3-6 Measured rail profiles at section km 10+450, between Globen and Gullmarsplan, together with the nominal BV50 rail profile, inclined 1:40. *A period of five years, corresponding to a traffic volume of 8.9 MGT, have passed between the two profiles. The radius is R=410 m.*

Despite the remarkable difference in curve radius, the difference between the amount of material removal on the outer rails in both curves is not so obvious. This is probably the effect of deliberate lubrication in the narrower curve, whereas the high rail in the wider curve is not lubricated. By comparison of the inner rail profiles it can be noticed that the area worn off in the narrower curve is significantly higher than the corresponding one for the wider curve. The difference is likely an effect of the smaller curve radius.

3.2 Vehicle

The investigated vehicle, A32, is a tram that is built in cooperation between formerly Adtranz in Sweden (today part of Bombardier Transportation) and Bombardier in Austria. It has been designed for low energy consumption, regenerating brakes, low levels of noise and 72 % low-floor area, as well as a high grade of recyclable materials [13]. The vehicle, that can be seen in Figure 3-7, is built for the ability of fast acceleration and with a maximum speed of 80 km/h. However, the ATP system (Automatic Train Protection) is not yet put into operation, so the maximum speed is limited to 50 km/h. This results in an average speed of 35 km/h, all stops included. The vehicle fleet is at the present time comprising 22 vehicles. Additional data can be seen in Table 3-3.

Figure 3-7 Stockholm tram vehicle A32 [13].

Table 3-3 Basic technical data of the vehicle A32 [13].

Length of vehicle	29.7 m
Width	2.65 m
Heigth	3.6 m
Car weight (empty)	37.6 t
Car weight (max loaded, 5 persons/m^2)	53.5 t
Seated passengers (max number)	78
Standing passengers (max number)	133

The main dimensions of the vehicle can be seen in Figure 3-8.

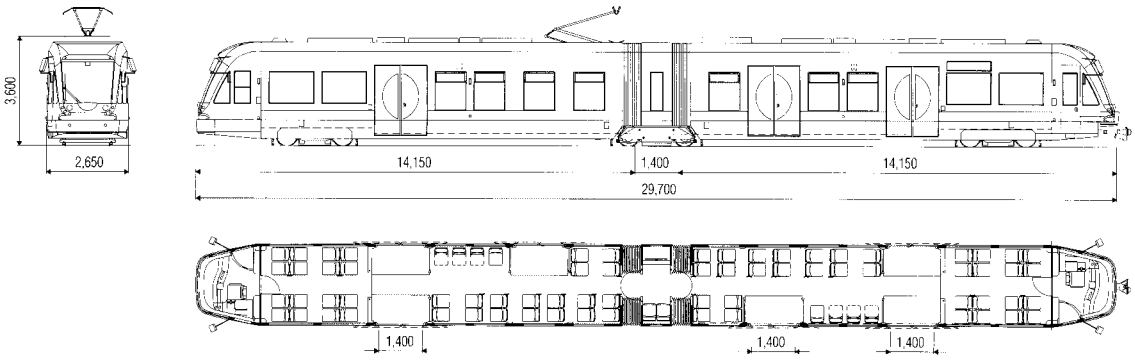

Figure 3-8 The A32 vehicle that operates on the light rail line Tvärbanan.

A32 is an articulated vehicle with two motor end bogies and one intermediate trailer bogie. The bogies are of compact design, which enables the low floor height. Each motor bogie has two conventional wheelsets and is equipped with two air cooled, self ventilated AC motors, additionally two mechanical brake discs and two magnetic track brakes. The trailer bogie, which is situated under the articulated part of the vehicle, is a relatively stiff bogie with four independently rotating wheels, including four mechanical brake discs and two magnetic track brakes [5].

A more detailed account of the components of the vehicle (bogies, wheelsets, suspensions, etc.) will be discussed in Chapter 4 in connection with the vehicle modelling.

3.2.1 Wheel profile

The vehicle consists of, as already mentioned, two different bogie types; a motor bogie and a trailer bogie. The wheels belonging to each bogie type differ from each other in design, but they have the same nominal wheel profile. The inclination of the tread on a non-worn (nominal) wheel profile is 1:40, where a short outer section at the field side is inclined 1:10. The inclination of the straight flange is nominally 62 degrees (1:1.88). The wheels are resilient with a nominal diameter of 630 mm and hydraulically pressed onto the axle. The nominal wheel profile can be seen in Figure 3-9.

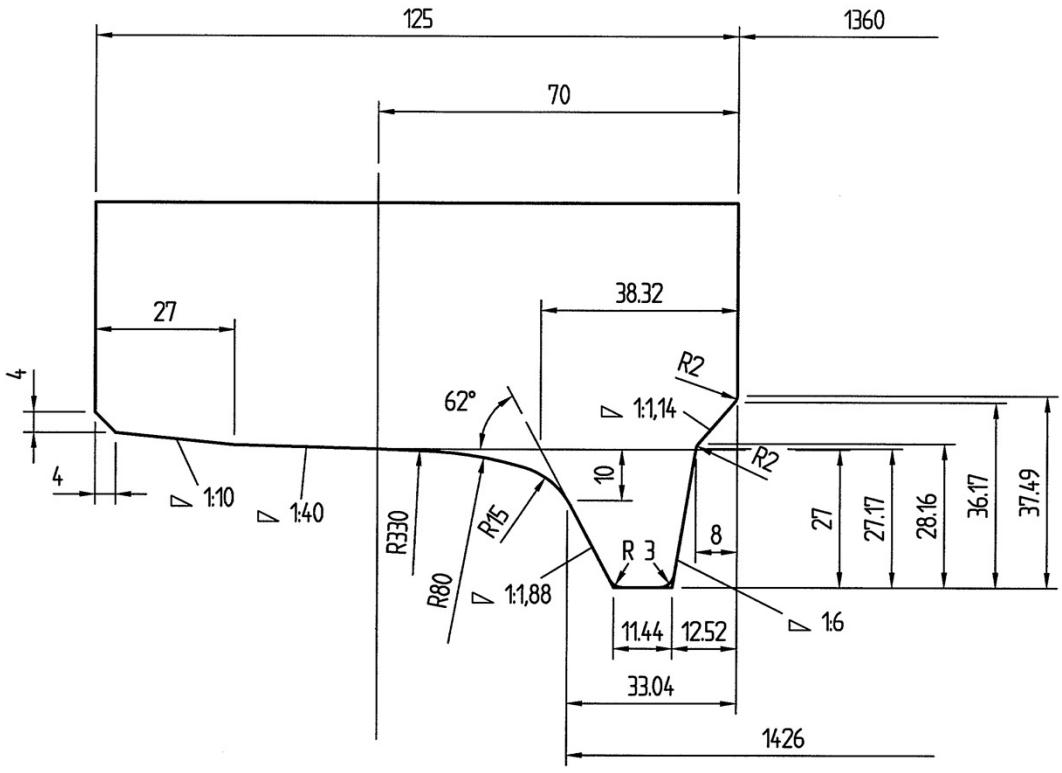

Figure 3-9 Nominal wheel profile of the vehicle A32.

4 Track-vehicle modelling and wear simulation

This chapter describes how the track and vehicle of Tvärbanan have been modelled for the simulations. The rail wear simulations are performed with the Swedish vehicle-track dynamics software GENSYS [6] in combination with a wear calculation program developed in MATLAB [23].

The procedure of the wear prediction tool can be divided roughly into four categories: *the simulation set design, track-vehicle simulations, wear calculations* and *updating of the rail profiles.* The flow chart of the present rail wear prediction program is shown in Appendix C, which can be useful when each category will be briefly presented in section 4.3-4.6.

4.1 Track model

There are a number of different track flexibility models, including the wheel-rail coupling, developed in the GENSYS program. The one applied in this work is the model shown in Figure 4-1, which is suitable for all kind of analysis, but especially when calculating dynamical vertical track forces [6].

The moving track model in Figure 4-1 contains four parts; ground (grd), "track" (trc; containing sleeper and part of ballast mass) and massless left and right rail heads (ral_l and ral_r). The wheels are connected to the rails through springs (knfr and knwr; two springs to enable two contact areas) and dampers (cnfr and cnwr, not shown in the figure) perpendicular to the contact area.

The rails have lateral and vertical degrees of freedom and are connected to the "track" through springs (kyrt and kzrt) and dampers (cyrt and czrt). The "track", on the other hand, is modelled with only a lateral degree of freedom and is connected to the ground through a lateral spring and damper (kytg and cytg). The ground is assumed to follow the designed track geometry (curvature etc.) and has thus no degree of freedom.

The nominal track geometry used in the model is applied according to Table 3-1. The transition curves are modelled as 80 metres long for the wider curves (R=300 m and R=410 m) and 50 metres for the narrower curves (R=85 m and R=130 m). The constant radius part of all curves is modelled as 100 metres long, cf. section 4.5.

Track irregularities

Track irregularities are deviations relative to the nominal track geometry and always present in rail traffic. They are included in the wear simulation, since they give rise to a realistic variation of the contact position and thus a smoother wear distribution. In GENSYS the track irregularities are described by the following four quantities: lateral, vertical, track gauge and cant irregularities. The track irregularities at Tvärbanan used in the model have been measured with the measuring car EM80 by Banverket [3], in August 2004, and a typical

example is shown in Figure 4-2. They represent a curve with a radius of approximately 400 metres, but are anyhow applied for all curves in this study. The track irregularities are centred around the nominal track gauge of 1435 mm, but according to measurements (cf. Table 3-1) it is appropriate to include a track gauge deviation of 5 mm in the model.

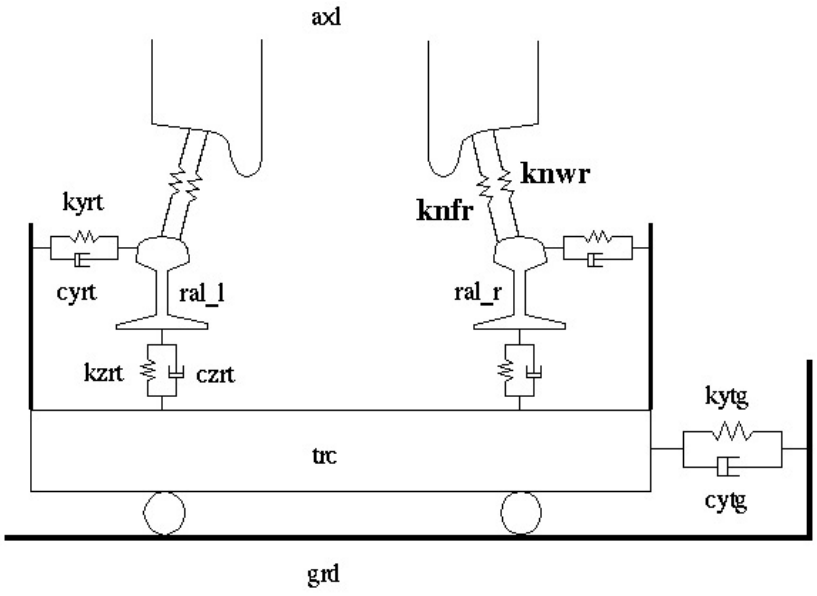

Figure 4-1 Track model used in the present GENSYS simulations [6]. *In GENSYS this model is called "pe1".*

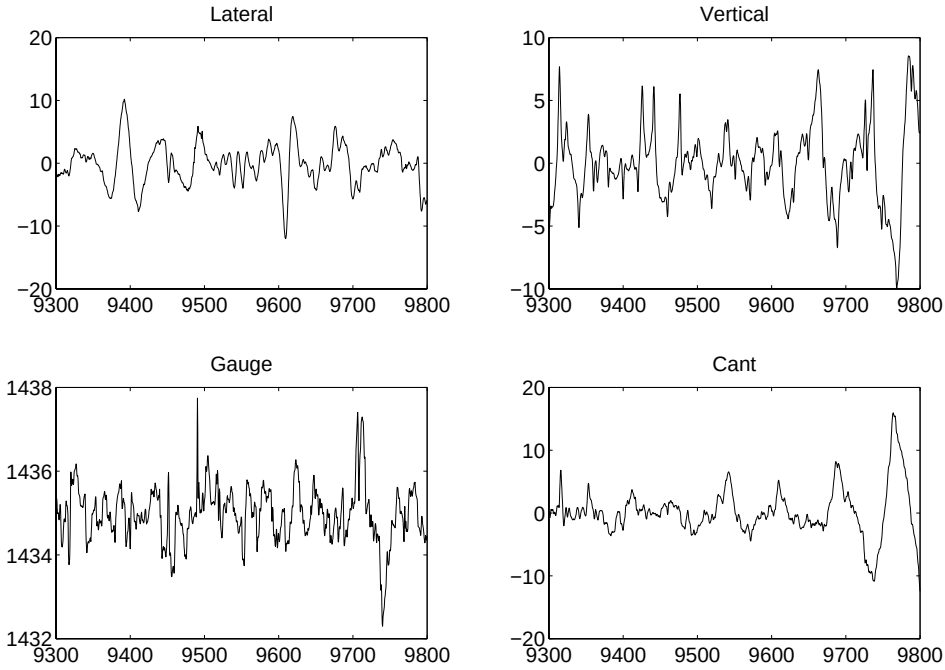

Figure 4-2 Measured track irregularities from car EM80, typically for a curve with R=400 m. *The four quantities lateral, vertical, gauge and cant. Dimensions in m on the x-axis and mm on the y-axis.*

4.2 Vehicle model

During normal traffic conditions it is sufficient to operate the railway line by single vehicles (see Figure 3-8 in the previous chapter), whereas two-vehicle trains are applied when the railway traffic is more intense (mornings and late afternoons). The wear simulations in this work are, however, performed with single vehicles only.

The components included in the vehicle are carbodies, bogie frames, bolster beams, wheelsets, primary and secondary suspensions. In the simulations the vehicle is represented by a multibody system (MBS) model with ridgid bodies, describing the mass properties, connected by different massless coupling elements, like springs and dampers.

The vehicle inertia data used in the model is shown in Table 4-1. The two longer end parts of the vehicle are similar and referred to as carbody 1, whereas carbody 2 is the short middle part, where the trailer bogie is situated (cf. Figure 3-8). The centre of gravity is defined as the height of the mass centre above the track plane (top of rail). J_{xx}, J_{yy} and J_{zz} are the moments of inertia with respect to the actual body's centre of gravity. All data in Table 4-1 refers to an empty vehicle without passengers.

Table 4-1 Inertia data for the vehicle A32 used in the model [20].

	Centre of gravity (m)	Mass (kg)	J_{xx} (kgm^2)	J_{yy} (kgm^2)	J_{zz} (kgm^2)
Carbody 1	1.500	12000	24000	230000	230000
Carbody 2	1.300	1700	2500	2300	1000
Motor bogie frame	0.300	2700	600	840	1400
bolster beam	0.445	350	220	10	230
wheelsets	0.315	2*700	260	20	250
Trailer bogie frame	0.270	1200	1000	300	1300
axle-boxes	0.315	4*220	4	5	4
wheels	0.315	4*200	6	10	6

Motor bogie

The motor bogie is shown in Figure 4-3 with the most prominent components indicated. Carbody 1 is connected to the bolster beam through a centre friction plate, modelled as stiffness couplings in all directions except in the yaw direction. However, in this direction a linear damping coupling is modelled. The bogie frame and bolster beam are interconnected by the secondary suspension, which consists of two progressive coil springs on each side of the bogie, but in the model they are composed to one stiffness coupling on each side of the bogie, linearized about the working point, regarding the normal load. The secondary suspension between bogie frame and bolster beam is, beside coil springs, modelled by the following components:

- The lateral suspension also includes one progressive bumpstop, modelled as an asymmetric, non-linear stiffness coupling, and one lateral hydraulic damper per bogie side, represented by a linear viscous damper.
- The vertical dampers at each bogie side are in the model represented by linear viscous dampers.
- The longitudinal stiffness consists of one traction rod per bogie side, linking the bogie frame and the bolster beam together. It is modelled as a linear coupling with both stiffness and damping properties.

The wheelsets and the bogie frame are interconnected by the primary suspension. It consists of two conical rubber components per axle box, with equal lateral and longitudinal stiffness. In the GENSYS model the primary suspension at each axle box is modelled as three linear springs, one for each direction, with both stiffness and damping properties. Note that the bogie frame is an inboard frame, i.e. the axle boxes of a wheelset are located between its wheels.

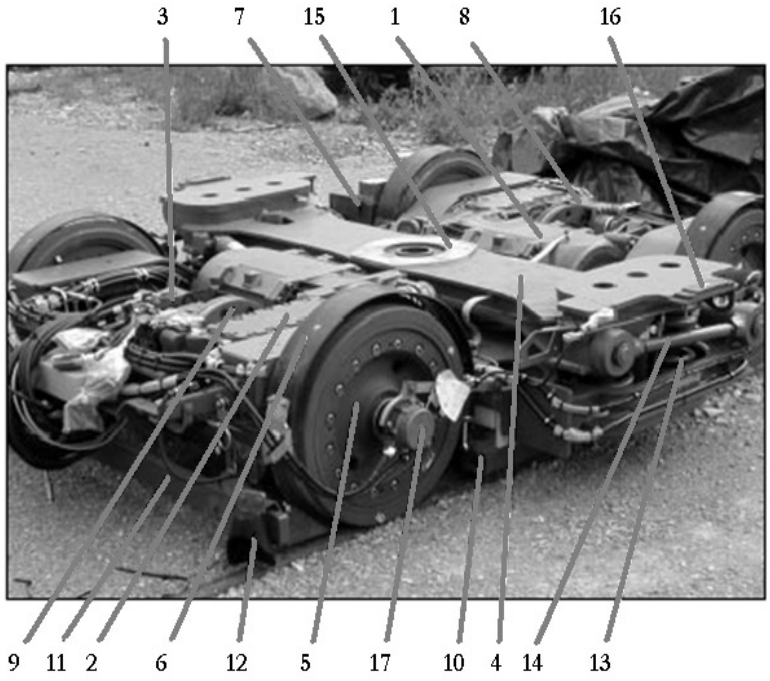

1. Motor	10. Magnetic track brake
2. Gear box	11. Life guard
3. Resilient axle coupling	12. Track cleaner
4. Bolster beam	13. Secondary suspension
5. Wheel	14. Traction rod
6. Mud guard	15. Centre friction plate
7. Two-step hydraulic operation unit	16. Lateral friction plate
8. Spring brake	17. Return current
9. Brake disc	

Figure 4-3 Motor bogie specified with the most prominent components [5].

Trailer bogie

The trailer bogie belonging to the A32 vehicle is shown in Figure 4-4. Carbody 2 and the trailer bogie are interconnected directly by the secondary suspension (no bolster beam). Each side of the trailer bogie is provided with two progressive coil springs as secondary suspension. In GENSYS they are, however, modelled as one stiffness coupling on each side of the bogie, linearized about the working point, regarding the normal load. The secondary suspension between bogie frame and carbody is, beside coil springs, modelled by the following components:

- The lateral suspension also includes one progressive bumpstop and one lateral hydraulic damper per bogie side, modelled as an asymmetric, non-linear stiffness coupling and a linear viscous damper, respectively.
- The vertical dampers at each bogie side are in the model represented by linear viscous dampers.
- The longitudinal stiffness consists of one traction rod per bogie side, linking the trailer bogie and the carbody together. It is modelled as a linear coupling with both stiffness and damping properties.

Each wheel of the trailer bogie is located at an axle box, which is connected to the bogie frame by the primary suspension, consisting of two resilient spherical bearings and a rubber block. They are modelled as one single equivalent linear tri-axial spring in the GENSYS model, with both stiffness and damping properties.

Other couplings

The three carbodies are connected to each other by articulation joints with friction plates. The joints are free to rotate in the pitch and yaw directions and are modelled as stiffness couplings in all other directions. In order to provide the vehicle with more lateral and pitch stability, there is a linkage on top of the vehicle roof, coupling the three carbodies together. It is modelled as a lateral linear stiffness and damping coupling in the GENSYS model. The effect of levelling the pitch angles between the carbodies is neglected.

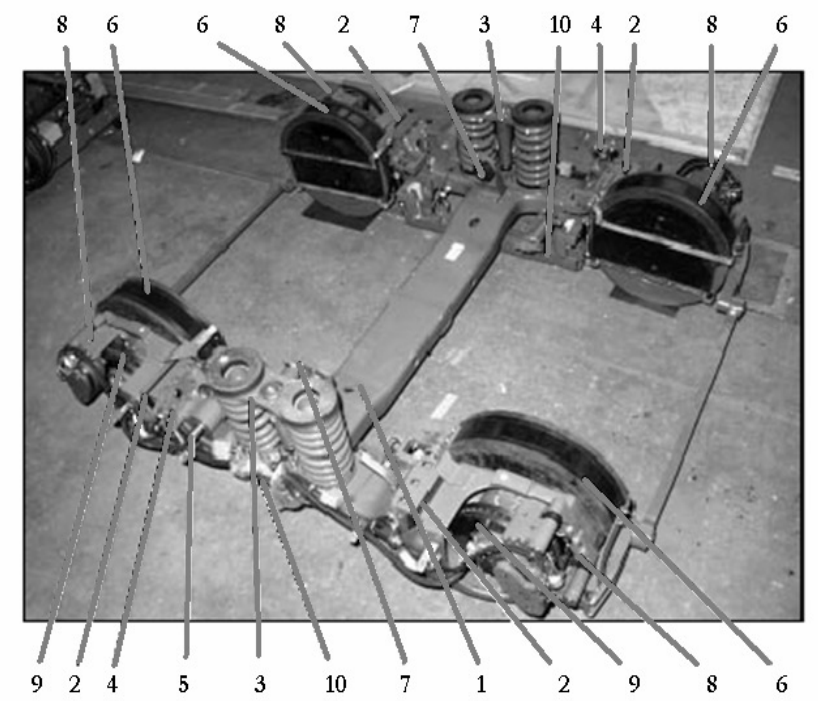

1. Bogie frame	6. Mud guard
2. Primary suspension	7. Lateral bumpstop
3. Secondary suspension	8. Spring brake
4. Liftstop	9. Brake disc
5. Linkage peg for traction rod	10. Magnetic track brake

Figure 4-4 Trailer bogie specified with the most prominent components [5].

4.3 Simulation set design

The general structure of the wear simulation methodology was presented in Section 2.1. The simulation set is thus designed by determining parameters such as *wheel profiles, vehicle speed* and *coefficient of friction*. The *vehicle type* parameter does not have to be taken into consideration, since there is only one single vehicle type that operates the line in this case. *Braking* and *acceleration* are also disregarded in the model; thus the effects of traction and braking in curves are not included in the present work. The other parameters valid for this application are, however, discussed below.

Wheel profiles

Three wheel profiles with different degree of wear have been included in the model in order to create a case as realistic as possible and to generate a smoother rail wear distribution. Firstly, a new, non-worn wheel profile is applied (wheel 1), cf. drawing of Figure 3-9. Secondly, a wheel profile that has run approximately 28 000 km is included in the model (wheel 2). It has been used consistently on the first axle of the vehicle, i.e. in a motor bogie. The third and last wheel profile derives from the previous wheel, but measured after 51 000 km of travelling distance (wheel 3). The three profiles are plotted together in Figure 4-5. On average, the wheels manage a travelling distance of approximately 50 000 km before wheel turning is required. However, none of the plotted wheel profiles has yet been turned.

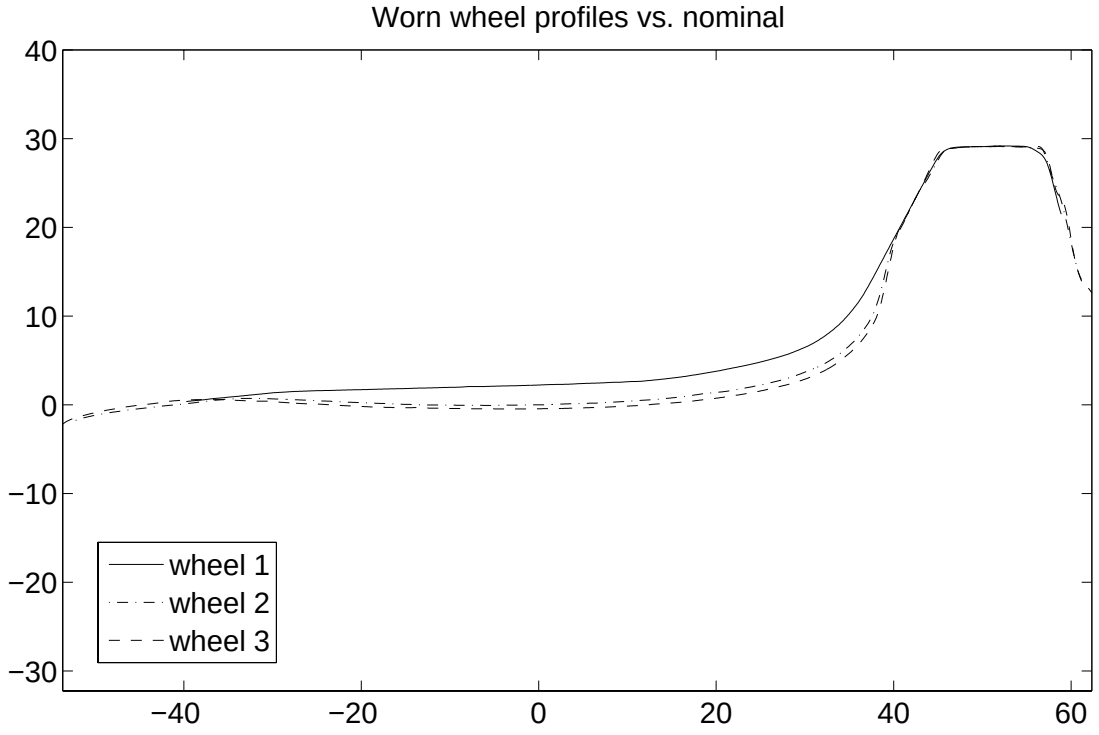

Figure 4-5 The three wheel profiles used in the model (after some smoothing). *The profiles are fitted at the top of the flange, at $x = 50$.*

It seems that the wheel profile wear is more extensive when the wheel is first put into use, but decreasing after a longer travelling distance. This is most likely an effect of the wheel and the rail needing some time to adapt their shapes to each other. It can be assumed that the rail profiles are also worn more in the beginning of their life.

In order to minimize discrepancies of the measured profile from the "real" profile, the wheel profiles have been manually smoothed before inserted in the model. All three profiles are equally weighted in the simulations (one third each) and are applied alternately at the three bogies in the vehicle in order to generate a smoother wear distribution. The simulations also become more realistic than with only one profile.

Vehicle speed

There is a permissible maximum speed of the vehicle, determined by the signal system (mentioned in Section 3.2) and, for each curve, the permissible cant deficiency. Thus, the vehicle speed is set to 50 km/h in all present curves, except in the narrowest one (R=85 m), where the speed is limited to 30 km/h.

Coefficient of friction

It is not obvious how the amount of wear is influenced by the coefficient of friction. The coefficient of friction can influence the dynamic behaviour of the vehicle, which in a wear point of view means the steering ability of the bogies and wheels. A higher coefficient of friction can result in higher creep forces, which result in a higher amount of wear. At the same time it can cause less sliding in the wheel-rail contact area, which, on the other hand, results in less wear. The relation between the coefficient of friction and the amount of wear is also dependent on whether the contact area is located at the head or the gauge face of the rail.

Measurements of the coefficient of friction were performed at Tvärbanan by SL before the opening of the light rail line. The results should, however, be regarded with caution, since the conditions during the measurements differ to a certain extent from the present conditions [21]. Due to differing contact environment, the coefficient of friction can vary considerably. The coefficient of friction used in the model varies between 0.10 and 0.20 for lubricated high rails and between 0.25 and 0.45 for non-lubricated rails. The middle values (0.15 and 0.35) are used in two thirds each in the model for the respective contact condition, whereas the surrounding values are applied as one sixth each. The model enables, when applicable, a difference between the coefficient of friction of the high and the low rail.

4.4 Track-vehicle simulations

The wheel-rail contact is modelled with Hertz' theory for the normal contact problem and with Kalker's simplified theory, implemented by the numerical algorithm FASTSIM, for the tangential contact problem (described in Chapter 2).

The rail and wheel profiles serve as input to a pre-processor in GENSYS called KPF (a Swedish acronym for Contact Point Functions), where the wheel-rail contact geometry functions are calculated. The functions are only valid for a particular wheel/rail combination and must, therefore, be computed for each unique combination in the simulation set, but also in every wear step, because of the changing rail profile.

Furthermore, the calculated KPF functions together with the simulation set and the vehicle MBS model are used as input to the time domain simulation program TSIM in GENSYS, where the equations of motions are solved for each time step, using a numerical integrator with adaptive time stepping. The KPF calculations and the time domain simulations are included in the flow chart of the wear prediction tool presented in Appendix C.

4.5 Wear calculations

The wear step loop is controlled by the main program *wpr.m*, including execution of KPF and TSIM as well as calculation of the wear depth (cf. Appendix C). After calculating the equations of motion in TSIM in each wear step, the contact mechanics and the wear depth are computed for selected time steps. The theory behind the wear calculations (Archard's wear model) has already been discussed in Chapter 2. From the main program *wpr.m* the subroutine FSIM_WPR.m is called. Here an extended version of the algorithm FASTSIM is used as a post-processor to the track-vehicle simulations to calculate sliding velocities and wear depth distribution over the slip area.

In order to obtain a more correct distribution of the sliding velocity, the contribution from the elastic surface deformation, mentioned in Section 2.3.2, is included in the model when calculating the sliding velocities.

Sampling for the wear calculations is made every second metre for all wheels in an interval of 100 metres in the circular part of the curve. The rail profile generated after one wear step is thus based on a sum of the wear for respective sampling points. The simulated tonnage for each wear step is thus a result of simulated axle passages multiplied by the axle load and samples.

Wear coefficient

The wear coefficient has been mentioned in Section 2.3.2, including a description of the regions of the wear map, depending on contact pressure, sliding velocity and the environment in the contact area, determined by temperature and lubrication.

Three different conditions in the wheel-rail contact can be described through the wear coefficient, namely a dry, naturally lubricated or deliberately lubricated environment. The

wear coefficient according to natural lubrication is scaled down from the dry condition by a factor of 5.5 and is applied in the larger curve (R=410 m) and all low rails. The other three curves (R=85 m, R=130 m and R=300 m) are deliberately lubricated on the high rails, where a wear coefficient reduced by a factor of 11 is applied. The scaling factors are estimated from field comparisons by Jendel [12].

4.6 Rail profile updating

When the rail wear distribution in each wear step has been calculated it is weighted according to certain criteria. The criteria that determine the weighting are axle passages and wear depth and are set in the wpr_input.m file to 3000 axle passages and 0.05 mm wear depth as maximum values.

Both the wear distributions and the updated rail profiles can in the model be chosen to be smoothed. It is performed in the file SMOOTH_D_W_WPR.m with a smoothing principle based on cubic interpolation. It is done in order to obtain physically reasonable rail profiles, but also to avoid interruption of the program if too rough and uneven wheel profiles are applied in the model. Smoothing of the rail profile should, however, be used rather carefully, since the interference of the profile can be too large. The smoothing procedure of the rail profile in this application, however, hardly gives any change of total wear, but instead a slight redistribution along the profiles.

5 Rail wear results

In this chapter the simulated rail wear results will be compared with the measurements of the rail profiles in the present curves at the light rail line Tvärbanan. Firstly, the actual rail wear at the four measuring sites will be presented.

5.1 Measured rail profiles

On the basis of the measurements it has been possible to calculate the area worn off relative to the nominal BV50 rail. By fitting two parts of the rail profiles, not exposed to wheel-rail contact, the rail wear can be determined. However, the initial rail profile is not measured at the corresponding measuring site, but derives from a drawing of the nominal BV50 rail. This leads to an uncertainty of the accuracy of the comparisons, since it turned out that the width of the profiles differs slightly. This resulted in problems when trying to fit the profiles together. The measured rail profiles (from September 2004) for each measuring site are plotted together with the nominal BV50 rail profile in Figure 5-1 to Figure 5-4.

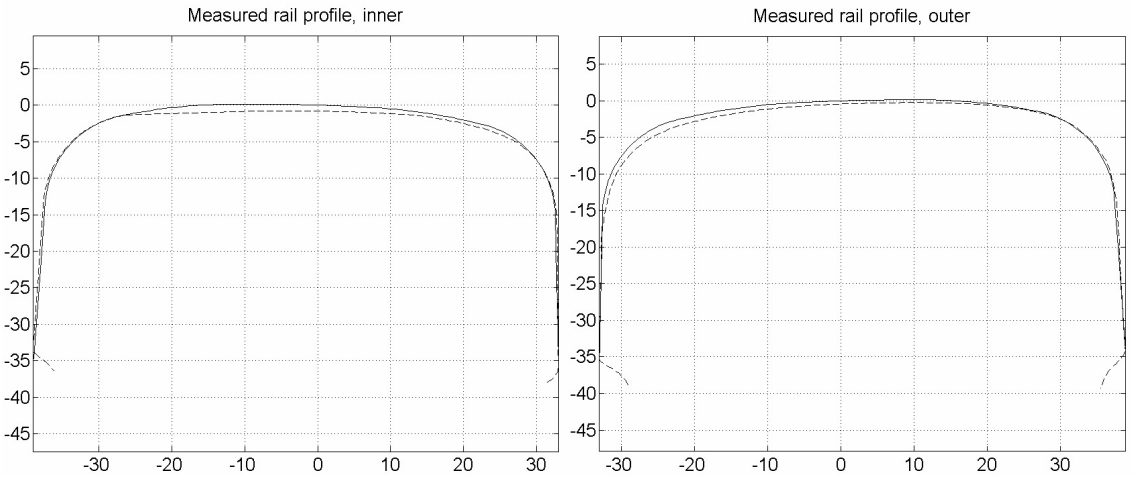

Figure 5-1 Measured rail profiles at section km 10+450 together with the nominal BV50 rail profile, inclined 1:40. *A period of five years, corresponding a traffic volume of 8.9 MGT, have passed between the two profiles. The radius is R=410 m. Measures in mm.*

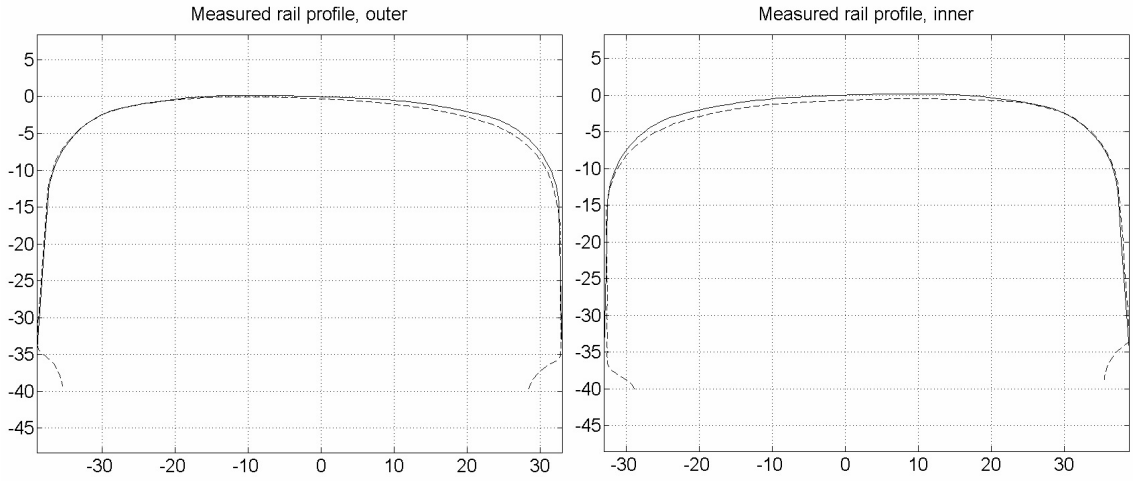

Figure 5-2 Measured rail profiles at section km 2+220 together with the nominal BV50 rail profile, inclined 1:40. *A period of four years, corresponding a traffic volume of 7.8 MGT, have passed between the two profiles. The radius is R=300 m. Measures in mm.*

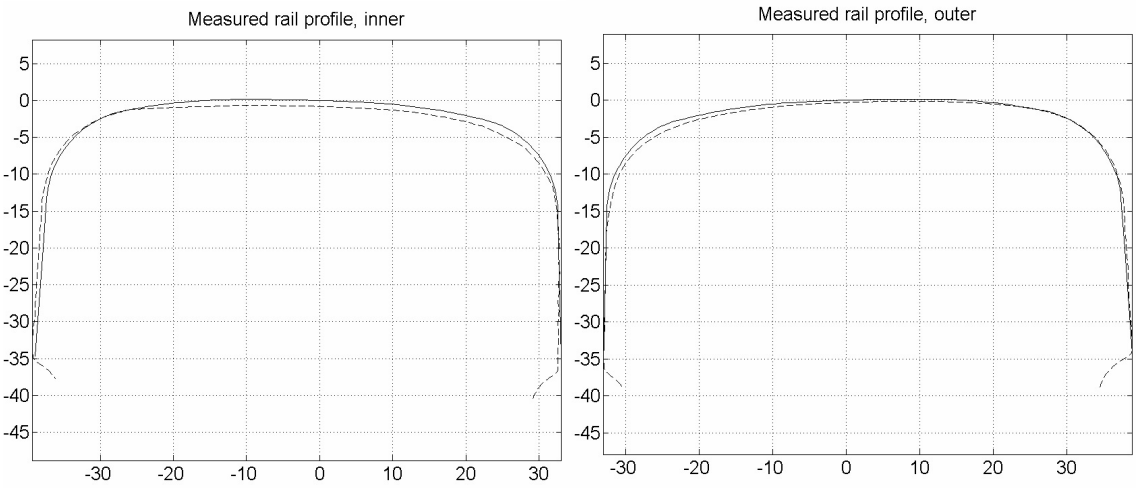

Figure 5-3 Measured rail profiles at section km 2+970 together with the nominal BV50 rail profile, inclined 1:40. *A period of four years, corresponding a traffic volume of 7.8 MGT, have passed between the two profiles. The radius is R=130 m. Measures in mm.*

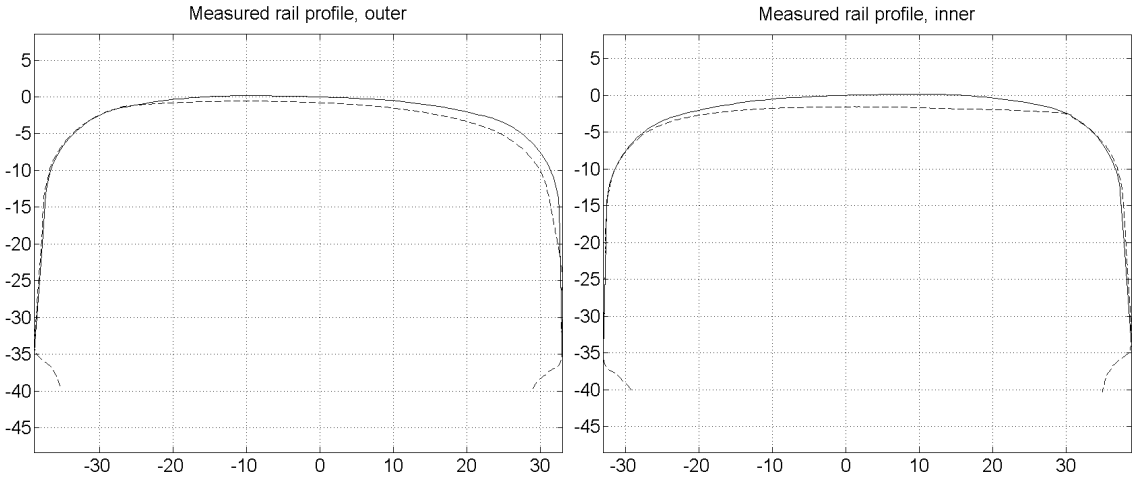

Figure 5-4 Measured rail profiles at section km 10+610 together with the nominal BV50 rail profile, inclined 1:40. *A period of five years, corresponding a traffic volume of 8.9 MGT, have passed between the two profiles. The radius is R=85 m. Measures in mm.*

When observing the shape of the worn rail profiles it can be noticed that the wear on the outer rails is more or less concentrated to the gauge face, whereas the inner rails are exposed to wear mainly at the rail head.

In Table 5-1 the calculated area worn off on both high and low rail is shown for the selected measuring sites at the northern track.

Table 5-1 Calculated area worn off on both high and low rail for the measured rail profiles.

Measuring sites	***R* (m)**	**Worn-off area, outer rail (mm^2)**	**Worn-off area, inner rail (mm^2)**	**Total traffic tonnage (MGT)**
10+450	410	35	37	8.9
2+220	300	30	42	7.8
2+970	130	33	48	7.8
10+610	85	65	74	8.9

According to the values of area worn off, the wear is more extensive on the inner rail, which in the narrower curves probably arises from the man-made lubrication of the outer rail. In the widest curve the difference between worn-off area of the outer and inner rail is not so obvious. It can also be noticed that the amount of wear increases as the curve radius decreases, except for the widest, non-lubricated curve.

5.2 Simulated rail profiles and comparison

For comparisons with the measured rail profiles, rail wear simulations have been implemented for each selected section. The simulated rail profiles are shown in Figure 5-5 to Figure 5-8.

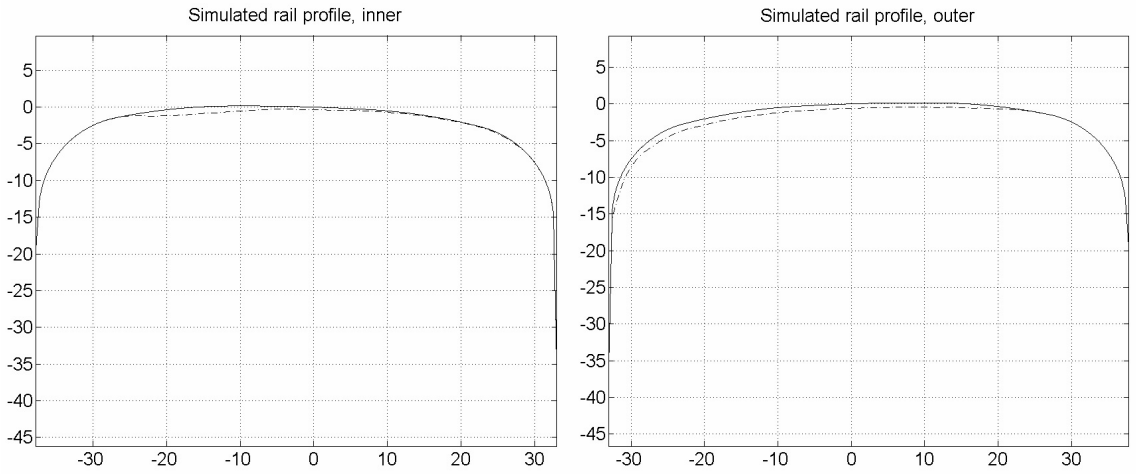

Figure 5-5 Simulated rail profiles at section km 10+450 together with the nominal BV50 rail profile, inclined 1:40. *The simulated traffic tonnage is 2.1 MGT and the radius is R=410 m. Measures in mm.*

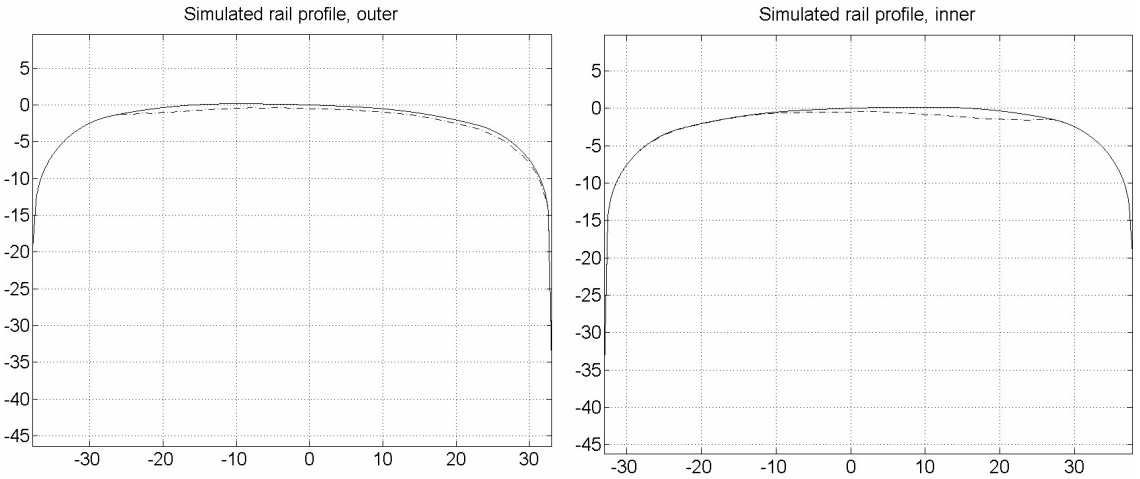

Figure 5-6 Simulated rail profiles at section km 2+220 together with the nominal BV50 rail profile, inclined 1:40. *The simulated traffic tonnage is 2.3 MGT and the radius is R=300 m. Measures in mm.*

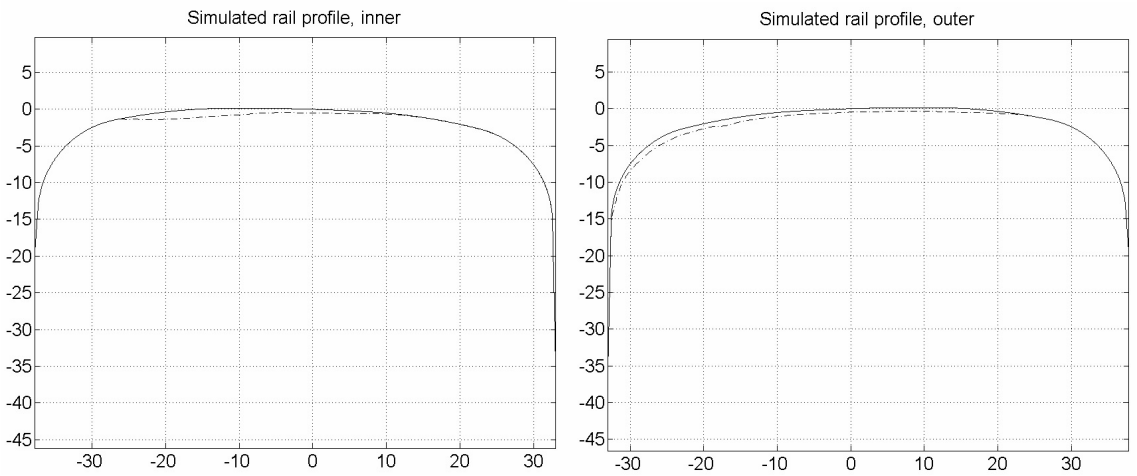

Figure 5-7 Simulated rail profiles at section km 2+970 together with the nominal BV50 rail profile, inclined 1:40. *The simulated traffic tonnage is 1.1 MGT and the radius is R=130 m. Measures in mm.*

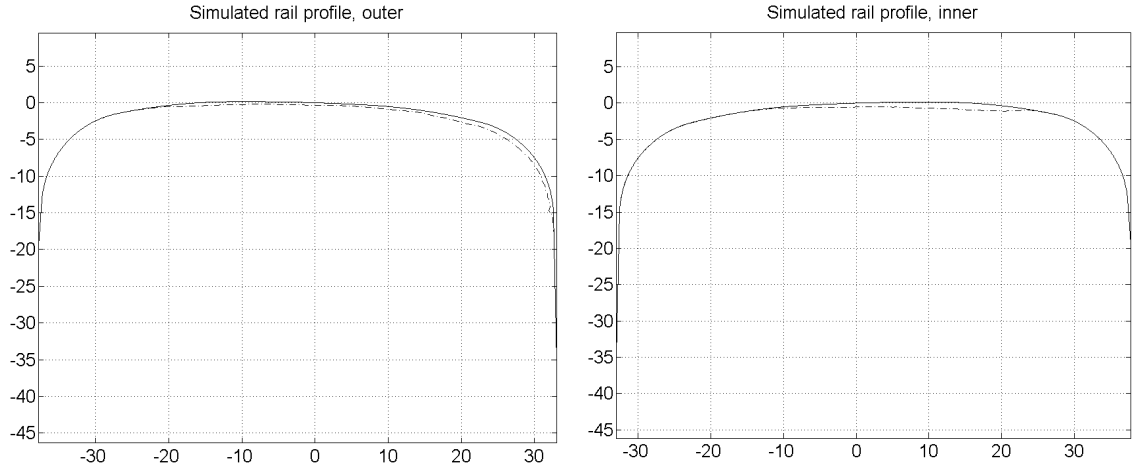

Figure 5-8 Simulated rail profiles at section km 10+610 together with the nominal BV50 rail profile, inclined 1:40. *The simulated traffic tonnage is 0.48 MGT and the radius is R=85 m. Measures in mm.*

The simulated rail wear is more extensive than the actual measured rail wear, in particular for the outer rails. Normally, the rail wear should be compared at the same amount of tonnage, but in this case it is more appropriate to compare the total tonnage at the same wear. The simulated area worn off is shown in Table 5-2 together with the traffic tonnage required. The simulation results are shown when the wear for the outer rail has reached the same amount as for the corresponding measured rail profile.

Table 5-2 Simulated area worn off at each measuring site.

Measuring sites	R (m)	Worn-off area, outer rail (mm^2)	Worn-off area, inner rail (mm^2)	Simulated tonnage (MGT)
10+450	410	35	19	2.1
2+220	300	30	27	2.3
2+970	130	33	25	1.1
10+610	85	27	22	0.48

The shape of the simulated rail profiles seems to agree fairly well with the measured profiles. The uncertainty in the comparisons of the rail profiles must, however, be regarded. It should also be noticed that the shape of the simulated inner rails differs from the measured ones, since the simulated area worn off has not attained the corresponding value as that of the existing profiles.

Note that the area worn off on the outer rail of the simulated rail wear for the narrowest curve (R=85 m) has not attained the same amount as that of the corresponding measured rail profile. The simulation work seems to be harder and even more time consuming to carry out the narrower the curve radius gets.

One way to reduce the simulated rail wear results is to use higher scaling factors for the wear coefficient. The work of improving the wear maps in order to make them valid for the actual contact conditions is in progress at the Royal Institute of Technology (KTH). Some indications have been made by Enblom particularly, that the scaling factors can be redefined for naturally and deliberately lubricated conditions to 7 and 21, respectively (instead of 5.5 and 11).

In the present work, a simulation with these higher scaling factors was implemented. This resulted in a decrease of rail wear that corresponded to the proportions of the original and the redefined scaling factors.

6 Conclusions and future work

Conclusions

A methodology for rail wear simulation has been introduced, where a simulation set has been selected, defining properties of the A32 vehicle that operates the light rail line Tvärbanan in Stockholm.

Archard's wear model has been used together with wear coefficents already determined by laboratory measurements. The wear coefficient has been reduced by a factor of 5.5 and 11 for natural and deliberate lubrication, respectively.

In the model it has been possible to use different values of the coefficient of friction on the high and low rail. On lubricated high rails the coefficient of friction has been varied between 0.10 and 0.20, whereas values between 0.25 and 0.45 have been applied for non-lubricated rails.

The wear distribution is weighted in each wear step according to maximum values of simulated axle passages and wear depth, corresponding to 3000 axle passages and 0.05 mm wear depth.

Due to some difficulties in obtaining physically reasonable simulated rail profiles, smoothing of both wear distribution and updated rail profiles has been applied in the simulation model, which resulted in a slight redistribution of the total wear along the rail profile.

The simulated wear rate is more extensive than the actual measured wear rate when comparing the profiles after the same amount of traffic tonnage, especially on the outer rails. The result was that comparisons of the traffic tonnage at the same wear were more appropriate.

However, the shape of the simulated rail profiles seems to agree fairly well with the existing rail profiles, regarding the uncertainty in the comparisons of the rail profiles. The wear on the outer rail is more concentrated to the gauge face, whereas the wear on the inner rail is located mainly at the rail head.

Future work

There are some actions that can be taken in order to improve the simulation results. The proposed improvements regarding the existing simulation model in GENSYS are the following:

- By increasing the simulation set with more wheel profiles of different shapes the real conditions of the wheel-rail contact will be better represented.
- A greater variation of the coefficient of friction in the contact area may result in a smoother distribution of the rail wear.
- Since some of the present curves are situated near stations it may be interesting to investigate to what extent braking and acceleration affect the rail wear.

- Since the simulations are so time consuming, it could be interesting to locate the most time demanding factors.
- It may be interesting for the owner of the track and vehicle (SL) to examine which vehicle parameters contribute the most to the rail wear, for instance the primary suspension properties.

The suggested improvements regarding the wear prediction tool are more extensive, demanding thorough investigations and developments.

- It is desirable to improve the wear maps, so that they are valid also for non-dry conditions.
- It is desirable to improve the wheel-rail contact model so that non-elliptical contact areas, as well as plastic material flow can be treated.

Appendix A - References

[1] Andersson E, Berg M and Stichel S: *Rail Vehicle Dynamics*, Text book, Division of Railway Technology, Department of Aeronautical and Vehicle Engineering, Royal Institute of Technology (KTH), Stockholm 2005.

[2] Archard J F: *Contact and Rubbing of Flat Surfaces*, Journal of Applied Physics, Vol 24, pp 981-988, 1953.

[3] Banverket: *Interpretation of Measuring Diagrams from EM50 and EM80* (in Swedish: Tolkning av Mätdiagram från EM50 och EM80), Edition 2, November 18, 1994.

[4] Banverket: *Rails - Requirements on New and Old*, (in Swedish: *Räler - Krav på Nya och Gamla*), BVF 524.1, 1998.

[5] Bombardier Transportation: *Product Description, Bogies, A32-2*, Document No. 903-BRA-0040, Revision 0, February 27, 1999. (Not public)

[6] DEsolver: GENSYS User's Manual, www.gensys.se.

[7] Enblom R: *Prediction of Wheel and Rail Wear - A Literature Survey*, TRITA - AVE Report 2003:27, Division of Railway Technology, Department of Aeronautical and Vehicle Engineering, Royal Institute of Technology (KTH), Stockholm 2003.

[8] Enblom R: *Simulation of Wheel and Rail Profile Evolution - Wear Modelling and Validation*, TRITA - AVE Report 2004:19, Licentiate Thesis, Division of Railway Technology, Department of Aeronautical and Vehicle Engineering, Royal Institute of Technology (KTH), Stockholm 2004.

[9] Esveld C and Gronskov L: *MINIPROF Wheel and Rail Profile Measurement*, Proceedings of the 2nd Mini Conference on Contact Mechanics and Wear of Rail/Wheel Systems, pp 69-75, Budapest, Hungary, July 29-31, 1996.

[10] Hertz H: *Über die Berührung zweier fester, elastischer Körper*, Journal für die rheine und angewandte Mathematik, Vol 92, pp 156-171, 1882.

[11] Jendel T: *Prediction of Wheel and Rail Wear - A Pilot Study*, TRITA - FKT Report 1999:03, Division of Railway Technology, Department of Vehicle Engineering, Royal Institute of Technology (KTH), Stockholm 1999.

[12] Jendel T: *Prediction of Wheel Profile Wear - Methodology and Verification*, TRITA - FKT Report 2000:49, Licentiate Thesis, Division of Railway Technology, Department of Vehicle Engineering, Royal Institute of Technology (KTH), Stockholm 2000.

[13] Johansson T, Peterson B E: *Tvärbanan - About the Return of the Light Rail in Stockholm*, (in Swedish: *Tvärbanan - Om Spårvägens Återkomst i Stockholm*), Statens Väg- och Transportforskningsinstitut (VTI), 2003.

[14] Kalker J J: *A Fast Algorithm for the Simplified Theory of Rolling Contact*, Internal Report, Delft University of Technology, Department of Mathematics, 1980.

[15] Kalker J J: *On the Rolling Contact of Two Elastic Bodies in the Presence of Dry Friction*, Ph.D Thesis, Delft, 1967.

[16] Kalker J J: *Review of Wheel-Rail Contact Theories*, ASME Applied Mechanics Division, Vol 40, pp 77-92, 1980.

[17] Kalker J J: *Three-Dimensional Elastic Bodies in Rolling Contact*, Kluwer Academic Publisher, Dordrecht, The Netherlands, 1990.

[18] Nilsson R: *On Wear in Rolling/Sliding Contacts*, TRITA - MMK Report 2005:03, Doctoral Thesis, Division of Machine Elements, Department of Machine Design, Royal Institute of Technology (KTH), Stockholm 2005.

[19] Personal communication with Adelpour F, *SL Infrateknik*, Stockholm.

[20] Personal communication with Bik U, *SL Infrateknik*, Stockholm.

[21] Personal communication with Olofsson U, *Department of Machine Design, Royal Institute of Technology (KTH)*, Stockholm.

[22] Shen Z Y, Hedrick J and Elkins J A: *A Comparison of Alternative Creep Force Models for Rail Vehicle Dynamic Analysis*, Proc of the 8th IAVSD Symposium, MIT, Cambridge, MA, pp 591-605, August 15-19, 1983.

[23] The Math Works: Using MATLAB, Version 6, Fifth Printing, 2000.

[24] Zobory I: *Prediction of Wheel/Rail Profile Wear*, Vehicle System Dynamics, Vol 28, 1997, Swets and Zeitlinger.

Appendix B - Notations

Latin letters

a	longitudinal semi-axis of the contact ellipse (m)
b	lateral semi-axis of the contact ellipse (m)
F_υ	total creep force in the contact area (N)
H	hardness (N/m^2)
J_{xx}	moment of inertia about longitudinal axis (kgm^2)
J_{yy}	moment of inertia about lateral axis (kgm^2)
J_{zz}	moment of inertia about vertical axis (kgm^2)
k	wear coefficient (-)
N	normal force (N)
p	pressure (N/m^2)
R	curve radius (m)
s	magnitude of sliding distance (m)
Δs	sliding distance in a contact area element (m)
Δt	time a contact area element is in contact with the rail (s)
u_η	lateral elastic displacement in the contact area (m)
u_ξ	longitudinal elastic displacement in the contact area (m)
$v_{vehicle}$	vehicle speed (m/s, km/h)
$\boldsymbol{v}_{slip}$	sliding velocity vector (m/s)
v_{slip}	magnitude of sliding velocity vector (m/s)
v_η	lateral sliding velocity (m/s)
v_ξ	longitudinal sliding velocity (m/s)
V_{wear}	volume of wear (m^3)
x	longitudinal coordinate direction
y	lateral coordinate direction
z	vertical coordinate direction

Greek letters

ζ	coordinate direction perpendicular to the contact plane
$\Delta\zeta$	wear depth for a contact area element (m)
η	lateral coordinate direction in the contact plane
η	local lateral coordinate in the contact area (m)
μ	coefficient of friction (-)
ξ	longitudinal coordinate direction in the contact plane
ξ	local longitudinal coordinate in the contact area (m)
υ	total creepage (-)
υ_η	lateral creepage in the contact plane (-)
υ_ξ	longitudinal creepage in the contact plane (-)
ϕ	spin (1/m)
ω	angular sliding velocity (rad/s)

Appendix C - MATLAB-GENSYS rail wear flow chart

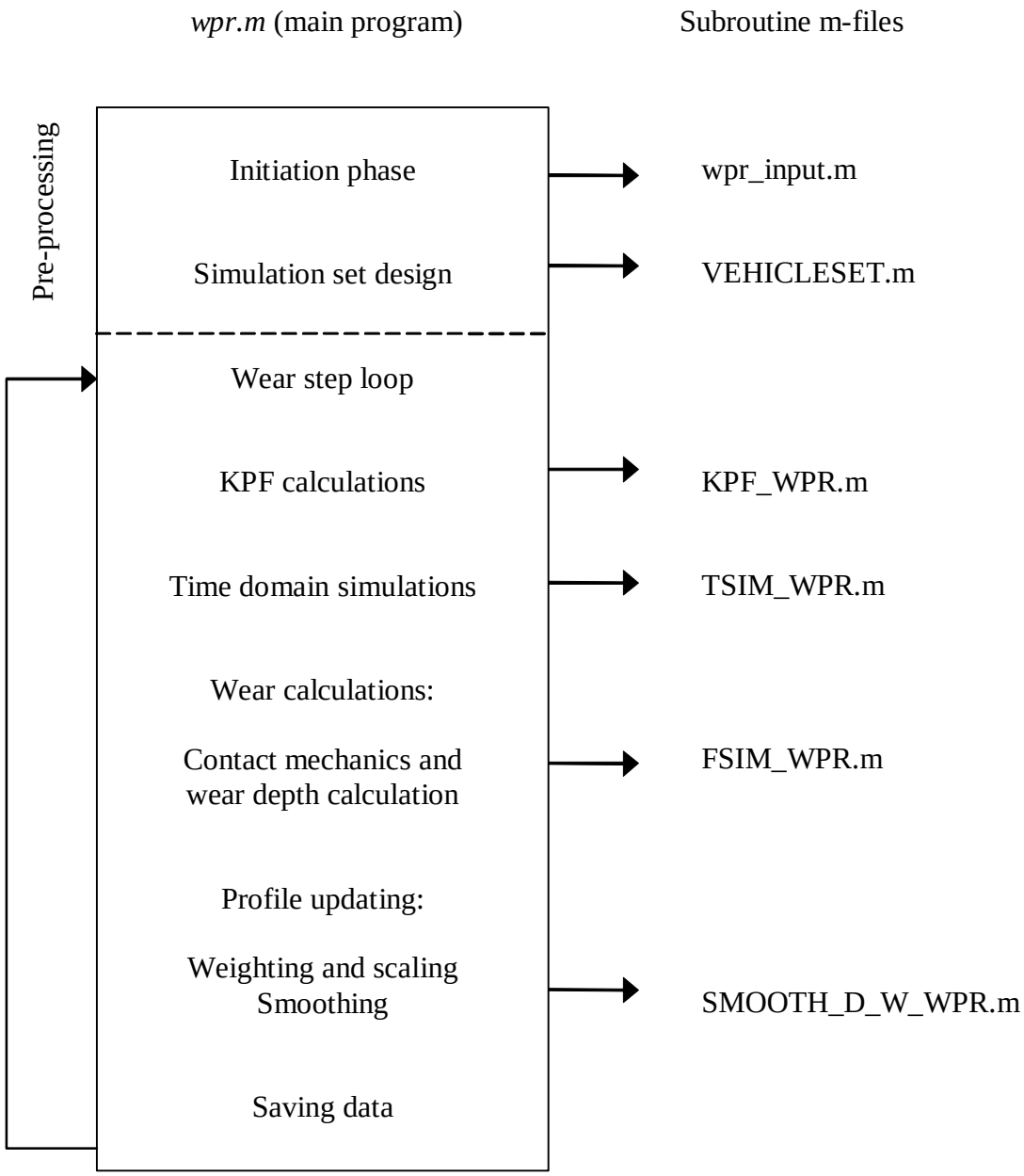

Figure C-1 Flow chart of the present wear prediction tool.